
Practical and scalable simulations of non-Markovian stochastic processes

Aurelien Pelissier^{1,2,*}, Miroslav Phan^{1,2,*}, Niko Beerenwinkel² and Maria Rodriguez Martinez^{1,†}

* Equal contribution

¹ IBM Research Europe, 8803 Rüschlikon, Switzerland

² Department of Biosystems Science and Engineering, ETH Zurich, 4058 Basel, Switzerland

† Corresponding authors. pel@zurich.ibm.com, mrm@zurich.ibm.com

Abstract

Discrete stochastic processes are widespread in natural systems with many applications across physics, biochemistry, epidemiology, sociology, and finance. While analytic solutions often cannot be derived, existing simulation frameworks can generate stochastic trajectories compatible with the dynamical laws underlying the random phenomena. However, most simulation algorithms assume the system dynamics are memoryless (Markovian assumption), under which assumption, future occurrences only depend on the present state of the system. Mathematically, the Markovian assumption models inter-event times as exponentially distributed variables, which enables the exact simulation of stochastic trajectories using the seminal Gillespie algorithm. Unfortunately, the majority of stochastic systems exhibit properties of memory, an inherently non-Markovian attribute. Non-Markovian systems are notoriously difficult to investigate analytically, and existing numerical methods are computationally costly or only applicable under strong simplifying assumptions, often not compatible with empirical observations. To address these challenges, we have developed the Rejection-based Gillespie algorithm for non-Markovian Reactions (REGIR), a general and scalable framework to simulate non-Markovian stochastic systems with arbitrary inter-event time distributions. REGIR can achieve arbitrary user-defined accuracy while maintaining the same asymptotic computational complexity as the Gillespie algorithm. We illustrate REGIR's modeling capabilities in three important biochemical systems, namely microbial growth dynamics, stem cell differentiation, and RNA transcription. In all three cases, REGIR efficiently models the underlying stochastic processes and demonstrates its utility to accurately investigate complex non-Markovian systems. The algorithm is implemented as a python library REGIR and supports the SBML format (<https://github.com/Aurelien-Pelissier/REGIR>).

Discrete stochastic processes [1] are prevalent in the study of a wide range of random phenomena in physics [2], biochemistry [3], epidemiology [4], finance [5] and meteorology [6]. To simplify their study, the Markovian assumption is usually postulated, under which, the system dynamics are memoryless, and therefore, the probability of any future occurrence solely depends on the present state of the system. Examples of Markovian systems are first-order reaction kinetics in biochemical networks, where the rate of reaction only depends on the present concentration of the reactant [7], or Brownian motion, where the displacement of the particle does not depend on its past displacements [8]. However, as the only memoryless continuous probability distribution is the exponential distribution, Markovian dynamics impose modeling inter-event times as exponentially distributed random variables.

Under the Markovian assumption, stochastic systems can

be simulated using exact algorithms, such as the seminal Gillespie stochastic algorithm [9, 10], which generates statistically correct trajectories of a stochastic system of equations with constant reaction rates. The Gillespie algorithm is computationally more efficient than alternative simulation methods such as agent-based models with constant time increments [11], and therefore, has been extensively used [12, 7, 13, 14, 15, 16].

However, real-world systems, and in particular systems characterized by hidden states, often exhibit memory, and therefore, generalizations have been sought. Hidden Markov models (HMMs) are an important class of Markov models that assume that the system dynamics depend on both observable and unobservable or *hidden* states [17]. At its essence, an HMM is a mixture model that encodes information about visible states (observations) and hidden states (the internal state of a system). HMMs have been extensively used to

model sequences, where the decomposition into observable and unobservable states captures dependencies between consecutive measurements in a sequence. Besides modeling biological sequence [18], HMMs have been used for speech recognition [19], economics [20], and climate modeling [21]. A drawback, however, is that HMMs require a larger number of parameters than simple Markov models and require computationally expensive learning or inference algorithms. Furthermore, the hidden intermediate states might be difficult to interpret phenomenologically.

Despite their elegance, the Gillespie algorithm and HMMs might not be good modeling choices for real-world systems exhibiting strong non-Markovian behavior, such as quantum devices [22], polymer reactions [23], molecular dynamics [24, 25, 26], biochemical reactions in single cells [27, 28], RNA transcription [29], neuronal firing [30], social interactions [31, 32], human activity patterns [33], or earthquakes [34], just to cite a few. In these cases, non-Markovian frameworks are necessary. However, non-Markovian stochastic processes are notoriously difficult to investigate, and exact analytical solutions have only been found for very simple problems, such as computing stationary levels of a one-gene system [35]. In most other cases, their study relies on expensive numerical simulations.

To facilitate the investigation of non-Markovian systems, several approximations have been developed, such as the non-Markovian Gillespie algorithm (nMGA). nMGA assumes that the inter-event times are exponentially distributed (as in the standard Gillespie) although the individual rates depend on the elapsed times of the processes [36]. The nMGA becomes exact in the limit of an infinite number of reactants ($N \rightarrow \infty$). However, the approximation error can become large for systems with few reactants. Furthermore, nMGA requires the recalculation of the instantaneous event rate of each process after each event occurrence, a procedure that is computationally expensive.

Alternatively, the Laplace Gillespie algorithm [37] provides an exact and computationally efficient algorithm to simulate systems where the inter-event times are a continuous mixture of exponentials, but the framework is applicable exclusively to monotone long tailed distributions. Finally, a recent paper by Großmann & al. [38] describes an approach to simulate non-Markovian propagation in connected contact networks such as Susceptible-Infected-Susceptible (SIS) models, but the approach is not applicable directly to more complex systems such as biochemical networks.

Here, we introduce REGIR (Rejection-based Gillespie for non-Markovian Reactions), a computational efficient algorithm to simulate non-Markovian dynamics with arbitrary inter-event waiting time distributions. Our approach exploits rejection sampling, a process where propensities that include undesired reactions are computed and subsequently rejected [39, 40, 13, 14]. REGIR addresses the existing limitations of the nMGA [36] and Laplace Gillespie [37]. First, it allows better approximation accuracy by reducing the simulation's time step Δt according to a user-defined threshold. Second, it considerably reduces the computational complexity and running time by computing only the reactions rates of the sampled reactants instead of all reactants, as nMGA and Laplace Gillespie does.

Thus, REGIR is capable of simulating systems characterized by non-exponential waiting-times with arbitrary precision, while maintaining the same asymptotic computational complexity as the traditional Gillespie algorithm (Figure 1).

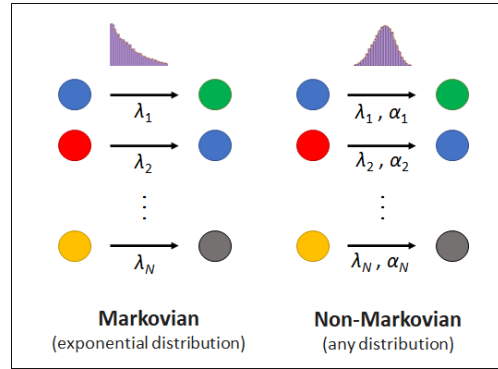


Figure 1: Diagram highlighting the differences between Markovian and non-Markovian stochastic models. **Left:** A set of reactants (blue, red, yellow,...) transforms into products through N reaction channels. The reactions are memoryless, i.e. inter-event times follow an exponential distribution with constant instantaneous rates λ_i . **Right:** In the non-Markovian case, inter-event times follow more complex distributions characterized by a larger number of parameters, in this case, λ_i, α_i . This results in instantaneous rates that depend on time.

REGIR is applicable to any distribution with finite instantaneous rates, which include the most commonly used distributions, e.g. the gamma, normal, log-normal or Weibull distributions.

This paper is structured as follows. We first introduce the REGIR algorithm and the standard parametrization of the distributions we will consider in the follow-up examples. We then demonstrate the use of REGIR on three significant biochemical applications, e.g. microbial growth dynamics, stem cell differentiation, and RNA transcription. Finally, we analyze the model's running time and approximation accuracy for different number of reactants.

Results

Rejection-based Gillespie for non-Markovian Reactions (REGIR). We consider a system of N renewal processes. In the standard Gillespie (SG) algorithm, each process is represented by a reaction channel that encompasses multiple reactants with the same reaction rate. When the number of reaction channels increases, the simulations become increasingly complex, which limits the applicability of SG to systems where reactants can be grouped into a few channels each one constituted by identical particles. In contrast, REGIR can simulate systems where each reactant obeys a distinct process with a different reaction rate. For each individual reactant, REGIR keeps track of the time elapsed since the last event, making the number of processes equal to the population size. In the SG, this would lead to a very large number of possible states and infeasibly long running times, however, REGIR minimizes the computational cost using the rejection approach described below.

Rejection sampling: We denote by t_j the time elapsed since the last event of the j th process ($1 \leq j \leq N$), and by $\lambda_j(t_j)$ the time-dependent reaction rate of the j th process. At each iteration, REGIR performs 4 steps, as described here:

- (i) Set λ_{\max} , the maximum reaction rate over all processes, such that:

$$\lambda_{\max} \geq \max_{j \in [1, N]} \lambda_j(t_j). \quad [1]$$

- (ii) Compute the time increment to the next event as in SG using λ_{\max} . Namely, a random variable is uniformly drawn from the interval $[0, 1]$, i.e. $u \in \mathcal{U}^{[0,1]}$. The time increment is computed as:

$$\Delta t = \frac{\ln(1/u)}{N \cdot \lambda_{\max}}. \quad [2]$$

- (iii) Select the process j that has produced the event. All processes have an equal probability of being drawn, and therefore, the probability of process j is:

$$p_j = \frac{1}{N}. \quad [3]$$

- (iv) Accept the process with probability p_{accept} , given by:

$$p_{\text{accept}} = \frac{\lambda_j(t_j)}{\lambda_{\max}}, \quad [4]$$

and update the reactants' population accordingly. If the process is rejected, the next event is set to an empty event, i.e. the reactant populations remain unchanged.

In the limit of $\Delta t \rightarrow 0$, which corresponds to $N \rightarrow \infty$ or $\lambda_{\max} \rightarrow \infty$ according to Eq. 2, the probability density function (PDF) of the inter-event times $\psi_j(t_j)$ of the j th process becomes:

$$\psi_j(t_j) = \lambda_j(t_j) \times \exp\left(-\int_0^{t_j} \lambda_j(\tau) d\tau\right). \quad [5]$$

The proof to Eq. 5 can be found in the Supplementary Information (SI, Section 1).

Main differences between REGIR and SG. There are several important differences between the REGIR and SG algorithms. First, SG simulates systems with constant reaction rates, i.e. stochastic systems that follow exponential distributions (SI, section 2). In contrast, REGIR allows for instantaneous rates for each process and reactant. Namely, REGIR keeps track of the time since the last event t_j for each process j , which enables the simulation of non-Markovian processes under the assumption that $\Delta t \approx 0$ [36]. Second, while SG keeps track of the rates of each reaction channel, REGIR only tracks the maximum rather than the individual rates of all processes at each time step. As we will show, this substantially reduces the computational cost of the algorithm [39], especially when the number of processes becomes large. Finally, while REGIR is an approximation algorithm, it can simulate processes with arbitrary accuracy. Indeed, λ_{\max} can be set at each iteration such that

$$\lambda_{\max} \geq f \cdot \frac{\lambda_0}{N}, \quad [6]$$

where λ_0 is the inverse of the mean inter-event time distribution, and f a factor defined by the user. Increasing f results in increased accuracy, at the cost of additional computational time. Thus, the optimal choice of f results from a compromise between the simulation accuracy and the computational cost. Throughout this article, we set $f = 30$ to achieve sufficient accuracy for the considered examples, and discuss the effect of choosing different values of f (Results Section and Fig. 5B).

Distributions. REGIR can simulate inter-event time distributions with finite instantaneous rates. However, this is not a real limitation, as distributions that do not verify this condition can be simulated by setting the rate to an arbitrary high value. Considering a renewal process with a probability density function (PDF) $\psi(t)$ and its survival distribution function (SDF) $\Psi(t) = \int_t^\infty \psi(t) dt$, the instantaneous rate function is defined as:

$$\lambda(t) = \frac{\psi(t)}{\Psi(t)}. \quad [7]$$

As an example, let us consider the Weibull distribution with PDF and SDF given by $\psi(t) = \beta t^{\alpha-1} \times \exp\left(-\frac{\beta t^\alpha}{\alpha}\right)$ and $\Psi(t) = \exp\left(-\frac{\beta t^\alpha}{\alpha}\right)$ respectively [41]. From these, we compute the instantaneous rate, $\lambda(t) = \beta t^{\alpha-1}$. Setting $\alpha = 1$, we recover the Markovian case with constant instantaneous rates. This is expected, as the Weibull distribution reduces to the exponential distribution when $\alpha = 1$. In the more general case, most distributions do not have instantaneous rates that can be written in simple analytical form (SI section 1B). However, it is always possible to compute numerically $\lambda(t)$ with arbitrary precision.

In this article, we demonstrate REGIR's simulation capabilities using the Weibull, gamma, normal and log-normal distributions as representative examples of distributions commonly used to represent biological systems. For consistency with prior work in stochastic simulations, each process in this article is parametrized by their mean inter-event time, $\frac{1}{\lambda_0}$ and a shape parameter. In the Section 1 of the SI, we explain how this alternative parametrization can be derived from the standard parametrization of each distribution. The shape parameter for the normal and log-normal distribution is denoted by γ and is defined as the standard deviation divided by the mean. Intuitively, γ represents a scale-invariant standard deviation. For the gamma and Weibull distributions, the shape parameter is denoted as α , which also represents the shape parameter of their standard parametrization. Thus, all inter-event time distributions in this article are parametrized with two variables, (λ_0, α) or (λ_0, γ) .

Application I: Microbial growth dynamics. As a first example, we describe microbial growth dynamics, more concretely, the inter-division times following microbial division and proliferation. Prokaryote cells must complete several steps, including DNA replication, chromosome segregation, and separation [42], before a new division can take place. Characterizing cell division with an exponential distribution implies that a cell has the largest probability to divide immediately after the cell division that created it, which is not physiologically possible. Instead, here we use REGIR to describe bacterial division using non-Markovian stochastic dynamics.

To identify the distribution that best fits bacterial inter-division times, we retrieved single-cell division times for *Bacillus subtilis* [43], *Escherichia coli* [44] and *Caulobacter crescentus* [45]. In all three cases, we found that the log-normal distribution provides the optimal fit as it minimizes the Earth Mover's Distance (EMD) [46] between the theoretical distribution and empirical data (SI, Table S1).

We test REGIR using population dynamics data of *Caulobacter crescentus* [45]. *Caulobacter crescentus* is a bacterium that divides asymmetrically into two morphologically

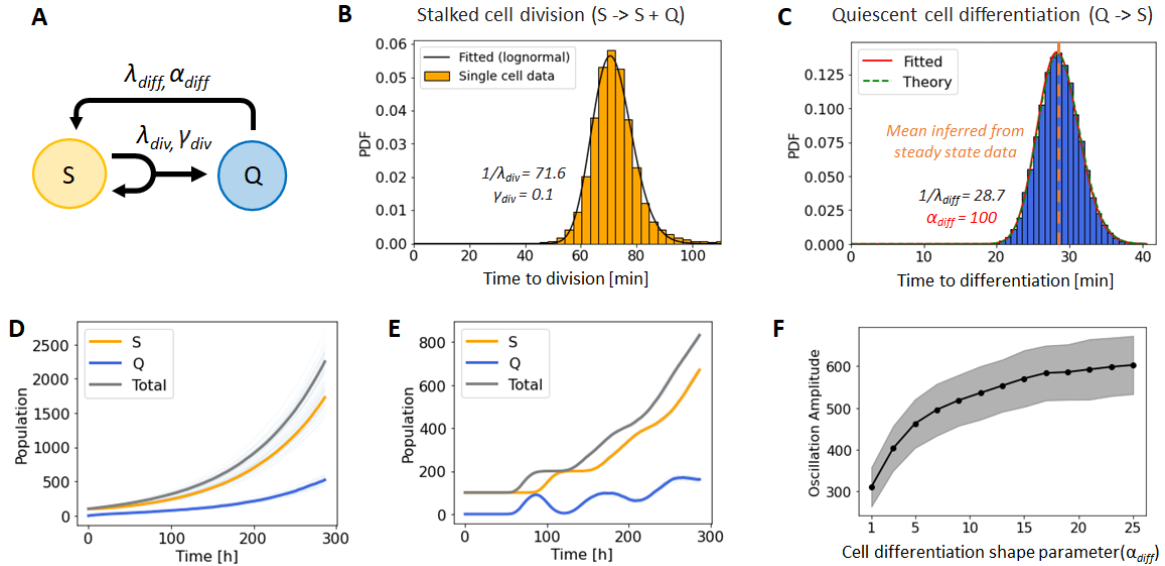


Figure 2: Microbial growth of *Caulobacter crescentus*. (A) Cartoon depicting the dynamics of microbial growth. A stalked cell S divides asymmetrically into another stalked cell and a motile quiescent cell Q that cannot divide further but can differentiate into a stalked cell. (B) Inter-event time distribution of stalked cell divisions using single-cell measurements from [45]. Data has been fitted to a log-normal distribution. The fitted distribution was later used in the REGIR simulation. (C) Simulated inter-event time of quiescent cell differentiation with a gamma distribution of shape parameter $\alpha_{diff} = 100$, chosen arbitrarily for the purpose of illustration (as there is no experimental data available). (D,E) Simulated population dynamics with an initial population of 100 stalked cells using Markovian processes and non-Markovian dynamics (REGIR), respectively, both with the same mean inter-event time, and with the inter-event distributions taken from subplots B & C for REGIR. (F) Evolution of the oscillation amplitudes as a function of α_{diff} while keeping all other parameters constant (as shown on subplots B & C). The black line shows the mean of 1000 simulations, and the shaded area corresponds to one standard deviation. The oscillations are quantified in terms of the root mean square deviation (RMSD) between the quiescent cells population dynamics and its exponential fit.

and functionally distinct daughter cells: a stalked cell (S) that is replication-competent, and a motile quiescent cell (Q) that cannot further divide but can differentiate into a stalked cell. Formally, we model the system with two reactions (Figure 2A,B,C):

- **Stalked cell asymmetric division:** $S \rightarrow S + Q$, modeled with a log-normal distribution of mean $1/\lambda_{div}$ and standard deviation $\gamma_{div} \cdot \lambda_{div}$ (optimal fit for the experimentally measured single cell data [45]).
- **Quiescent cell differentiation:** $Q \rightarrow S$, modeled with a gamma distribution of mean $1/\lambda_{diff}$ and shape parameter α_{diff} . The characterization of quiescent cell differentiation into a stalked cell is experimentally challenging [47], and currently, there is no data to infer the shape of the inter-event time distribution. Hence, we represented this process with a gamma distribution, as it can model more diverse shapes than a log-normal distribution – a gamma distribution interpolates well between long-tailed ($\alpha_{diff} < 1$), exponential ($\alpha_{diff} = 1$) and normal-like ($\alpha_{diff} \gg 1$) distributions.

For the purpose of comparison, we also simulate a Markovian model with the same mean inter-event times λ_{div} and λ_{diff} as REGIR (Figure 2D). Interestingly, simulations based on exponential waiting times results in faster population growth than the simulations based on log-normal and gamma-distributed waiting times (Figure 2E). This disparity is a known analytical result for symmetric division ($A \rightarrow 2A$), in which the mean division time of single cells, $\mu = 1/\lambda_{div}$, is different from the mean doubling time of the population t_2 . For example, in the case of inter-division times following a gamma distribution of parameters $(\lambda_{div}, \alpha_{div})$, the mean population

doubling time is given by (SI, Section 3A)

$$t_2 = \mu \cdot \frac{\ln(2)}{\alpha_{div} (2^{1/\alpha_{div}} - 1)}, \quad \text{with } \mu = \frac{1}{\lambda_{div}} \quad [8]$$

where $\alpha_{div} = 1$ recovers the Markovian case, i.e. $t_2 = \mu \ln(2)$, and $\alpha_{div} = \infty$ the deterministic case, $t_2 = \mu$. This simple example highlights the importance of correctly accounting for possible non-Markovian processes when studying population dynamics.

In the case of *Caulobacter crescentus*' asymmetric division, it was previously shown analytically that both quiescent and stalked cells grow exponentially with the same rate k for any distribution [48]. Still, the growth rate k generally does not have a simple analytical form (SI, Section 3B). In Figure S3, we leverage REGIR to show how the growth rate varies for different distribution parameters. As expected, changes in the mean of the distribution have a much larger impact on the growth rate than changes in the shape parameter. Nevertheless, the shape parameter can affect the growth rate by more than $\sim 20\%$, highlighting the importance of properly accounting for it.

After fitting the model parameters with experimental data from [45], consisting of single-cell measurements of division times, as well as steady-state cell populations ratios of stalked and quiescent cells at 31°C , we were able to constrain 3 out of 4 model parameters. However, we were not able to constrain α_{diff} as the data only provides information about steady-state levels for quiescent cell differentiation – for technical reasons, the direct experimental characterization of quiescent cell differentiation is challenging [47]. As previously shown [48], the deterministic modeling of quiescent cell differentiation reveals transient oscillations, as the initial populations are highly synchronized and differentiate

at the same time. Stochastic models should partially smooth these transient oscillations, as division and differentiation occur probabilistically, which results in the gradual loss of synchronization. However, we see that in the Markovian case the oscillations have completely disappeared (Figure 2D), i.e. the exponentially distributed inter-event times fully mix division and differentiation times destroying the synchronization. Opposed to this, the non-Markovian simulation still shows transient oscillations (Figure 2E). Interestingly, the amplitude of the quiescent cell population oscillations increases as the variance of the inter-event differentiation time of stalked cells reduces (Figure 2F). We note that with our parametrization, α_{diff} inversely correlate to the variance of the distribution through the relation $\text{Var} = 1/(\alpha_{\text{diff}}\lambda_{\text{diff}}^2)$.

Application II: Stem cell differentiation. Another interesting application for REGIR is stem cell differentiation, the process by which specialized cells are formed from stem cells [49]. Stochastic fluctuations in key transcription factors play important roles in the early stages of differentiation [50], however, it is less clear whether the progress in cellular differentiation is also an intrinsically stochastic process, or a carefully orchestrated mechanistic process where cells transition through a continuum of intermediary meta-stable states. The latter hypothesis would explain the observed precise regulation of differentiation processes at the single-cell level.

From a modeling point of view, transitions between functional cell types can be described as a stochastic process with *memory*, where memory allows cells to keep a record of their current functional identity before progressing to the next. Such processes can be described using non-Markovian stochastic dynamics. While the mean inter-event time ($1/\lambda_0$) is the most readily available parameter, the shape of the distribution (e.g. the variance, Fano factor, etc.) is equally important in the study of cell differentiation. However, measuring distribution shapes requires tracking differentiation times in single cells, which is experimentally challenging. Easier to obtain are the population dynamics of the different cell types, e.g. the fraction of cells in each sub-population at different time points. Here, we demonstrate how REGIR can infer the shape of the single-cell inter-event time distribution directly from the cell population data.

Concretely, we use REGIR to investigate the stochastic cellular differentiation of mouse embryonic stem cells (ESC) as they differentiate along the neural lineage [28]. Cells are profiled at the single-cell level at 3 different stages of differentiation, including embryonic stem cells (ESC), epiblast-like (EPI) states, and neuroprogenitor cells (NPC). The data was originally modeled using a hidden Markov model (HMM) [17], which allows for the existence of hidden variables, i.e. microstates with distinct genetic and molecular profiles mapping to the 3 cellular macrostates, ESC, EPI, and NPC. Fitting the experimental data to this model required the definition of 19 or 20 microstates, depending on the cell line used in the experiment. Moreover, as HMMs can have different emission and absorption rates for each microstate, the final number of parameters might be significantly large. Interestingly, however, the authors assumed all transitions between the hidden and observable states had the same rate, which in practice resulted in modeling the inter-event distribution as an Erlang distribution of mean λ_0 and shape parameter k .

REGIR accurately reproduces the stochastic differentiation dynamics in a simpler manner and does not require the definition of any microstate. Namely, we summarize stem

cells dynamics using only two stochastic reactions (Figure 3):

- **ESC** \rightarrow **EPI**, modeled with a gamma distribution of parameters (λ_1, α_1) .
- **EPI** \rightarrow **NPC**, modeled with a gamma distribution of parameters (λ_2, α_2) .

We minimized the root mean square deviation (RMSD) between the experimentally measured cellular populations at each cellular state and time point and two different REGIR simulations: (i) a non-Markovian simulation using two gamma distributions of parameters λ_1, α_1 , and λ_2, α_2 , which resulted in an RMSD of 0.35; and (ii) a Markovian simulation using SG with parameters λ_1 and λ_2 , which resulted in a substantially larger RMSD of 2.1 (\sim an order of magnitude larger). The better fit provided by the non-Markovian REGIR simulation is also evident in Figure 3, where we compare the experimental data with the Markovian and non-Markovian REGIR simulations.

We repeat the same analysis by modeling the differentiation process with other distributions, including the normal, log-normal, and Weibull distributions. The optimal parameters and RMSD are shown in SI (Section 4 and Table S2). Interestingly, the Weibull distribution resulted in a worse fit (RMSD = 0.69) than the gamma (RMSD = 0.35), normal (RMSD = 0.38), and log-normal (RMSD = 0.39) distributions. We note that the optimal distribution might depend on data preprocessing choices. For instance, an inverse sigmoid (or logit) transformation is sometimes applied to proportion and percentage data to expand the ends of the distribution (data points close to 0 and 1), such as there is a nearly linear relationship between $\text{logit}(p)$ and p . For logit-transformed data, the gamma distribution provides the optimal fit in terms of RMSD, while the log-normal distribution is optimal for non-transformed data. In both cases, however, the log-normal, normal, and gamma distributions achieve similar low RMSD values, likely because of the qualitative similarity between these distributions, while the Weibull distribution performs significantly worse.

As a gamma distribution with an integer shape parameter k corresponds to the sum of k independent exponential variables of the same mean (also known as the Erlang distribution), we can conclude that the hypothesis of stem cells going through several microstates during differentiation as proposed in the original study [28] is indeed a valid interpretation.

Application III: RNA transcription. Transcription is the process by which a gene's DNA sequence is copied (transcribed) to produce mature RNA (mRNA) molecules. Briefly, after RNA polymerase binds to the promoter region of the gene, a nascent RNA molecule is produced and progressively elongated until the full gene has been transcribed. The nascent RNA matures into an mRNA molecule, which is used to produce proteins (translation). mRNAs progressively degrade at an approximately constant rate. Advances in real-time measurement of single-cell dynamics have revealed the stochastic nature of gene transcription [51] and sparked interest in building stochastic models to simulate this process [52, 29].

A popular model to describe RNA transcription involves a promoter switching between an ON and an OFF state at constant rates, which leads to non-Poissonian mRNA fluctuations and predicts well the bursty mRNA expression observed experimentally [53]. This model, commonly referred to as

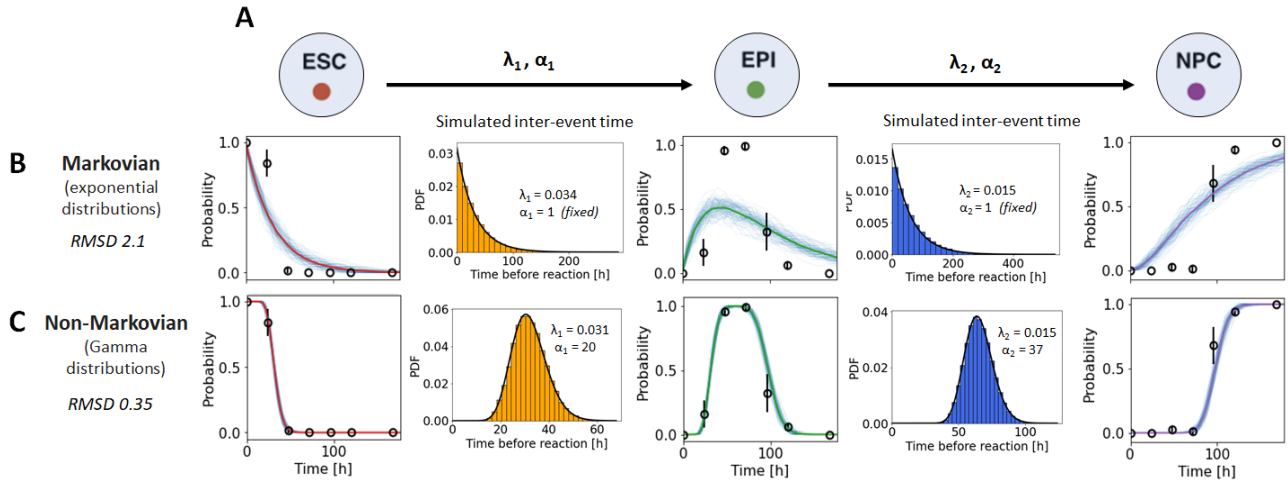


Figure 3: (A) Mouse stem cells at 3 different stages of differentiation. From the ESC stage, the cell may differentiate into EPI which in turn may differentiate into NPC. The inter-event time associated with these 3 stages of cellular differentiation are modeled using either (B) two exponential or (C) two gamma distributions. The average root mean square deviations (RMSDs) between the simulated and measured data at each time point and for each cell type are indicated for both models. The Markovian case was fitted by fixing the shape parameter $\alpha_1 = \alpha_2 = 1$ (which corresponds to an exponential distribution). The black circles and error bars represent the mean and standard deviation of the stem cell populations measured at different time points [28], and the solid lines depict the population dynamics obtained after averaging 1000 REGIR simulations with the parameters that minimize the RMSD. Each single simulation is depicted with a narrow blue line. The simulated inter-event time distributions obtained after parameter optimization are plotted in orange and blue, for the first and second differentiation respectively.

the *two-state* or *telegraph model*, has been widely adopted in the literature as the standard model of stochastic mRNA dynamics in eukaryotic cells. It has been extensively studied analytically [54] and used to infer RNA kinetics parameters of thousands of genes in both mouse and human fibroblasts, directly from single-cell RNA-sequencing data [55, 56].

Still, there is a large body of experimental evidence showing that the distribution of molecule fluctuations is typically non-Poisson [29], and hence, non-Markovian descriptions are necessary. Importantly, non-Markovian simulations can clarify how changes in the shape parameters of the underlying molecular processes modulate mRNA expression levels. To investigate this, we model the RNA transcription process with 4 reactions as follows (Figure 4A):

- **Promoter activation and deactivation:** $G_{\text{off}} \xrightarrow{\lambda_{\text{on}}, \alpha_{\text{on}}} G_{\text{on}}$ and $G_{\text{on}} \xrightarrow{\lambda_{\text{off}}, \alpha_{\text{off}}} G_{\text{off}}$. A promoter continuously switches between OFF and ON states, with the inter-event times following gamma distributions of parameters $(\lambda_{\text{on}}, \alpha_{\text{on}})$ and $(\lambda_{\text{off}}, \alpha_{\text{off}})$.
- **RNA production:** $G_{\text{on}} \xrightarrow{\lambda_{\text{prod}}, \alpha_{\text{prod}}} G_{\text{on}} + \text{mRNA}$. When the promoter is ON, a mature mRNA can be produced by the RNAP enzyme (initiation and elongation stages). We model this process with a gamma distribution of parameters $(\lambda_{\text{prod}}, \alpha_{\text{prod}})$.
- **RNA degradation:** $\text{mRNA} \xrightarrow{\lambda_{\text{deg}}} \emptyset$. Since experiments show that mRNA decay typically follows first-order kinetics [57], we model this process with an exponential inter-event time distribution.

Without loss of generality, all rates are given in units of λ_{deg} (i.e. $\lambda_{\text{deg}} = 1$), which is common practice in RNA transcription studies [55, 54].

To emphasize the relevance of non-Markovian dynamics in RNA transcription, we leverage time-resolved mRNA profiles after stimuli by the epidermal growth factor (EGF),

measured with real-time quantitative PCR (qPCR) [58]. Interestingly, several genes, e.g. CREG1, DDB2, SLC7A5, NFYC, NR4A1, PTGS2, displayed oscillations after stimulation in their mRNA expression levels that could not be replicated with the Markovian model (Figure 4B, SI section 5B). In contrast, after fitting the distribution parameters from experimental data, REGIR was able to reproduce the oscillations. Interestingly, the oscillation period T is directly related to the activation and deactivation rates with $T = 1/\lambda_{\text{on}} + 1/\lambda_{\text{off}}$, and the *decay* in the oscillation amplitude can be approximately fitted by adjusting the shape parameters α_{on} and α_{off} (SI, Section 5A). This pattern was observed in several of the measured genes [58], and supports the hypothesis that gene activation and deactivation in the two-state RNA transcription model are not well described with Markovian dynamics (SI, Section 5B) [59].

Our simulations show that the steady-state mRNA distribution can be significantly affected by the shape parameter of the underlying inter-event time distributions. Indeed, in the bursty regime, which is the regime where the majority of genes are actively being transcribed into mRNA, and roughly corresponds to $\lambda_{\text{off}} > \lambda_{\text{on}}$ and $\lambda_{\text{prod}} \gg \lambda_{\text{off, on}}$ [29], the shape parameters α_{on} and α_{off} significantly affect the steady-state mRNA distribution. For example, in the case of Figure 4C, there is a high probability of measuring an mRNA count of zero in the Markovian case ($\alpha_{\text{on}} = 1$, $\alpha_{\text{off}} = 1$), while this probability becomes very small for ($\alpha_{\text{on}} = 10$, $\alpha_{\text{off}} = 10$).

In order to determine the parameters that most contribute to the variance in the model's output, we perform a Sobol variance-based sensitivity analysis [60]. It has previously been shown that the mean mRNA distribution in steady-state only depends on the mean inter-event time distribution [35], and thus, it is not affected by the shape parameters (SI, Section 5C). Therefore, we quantify the model sensitivity in terms of the coefficient of variation (CV = std / mean) of the mRNA steady-state distribution (Figure 4D). Our analysis

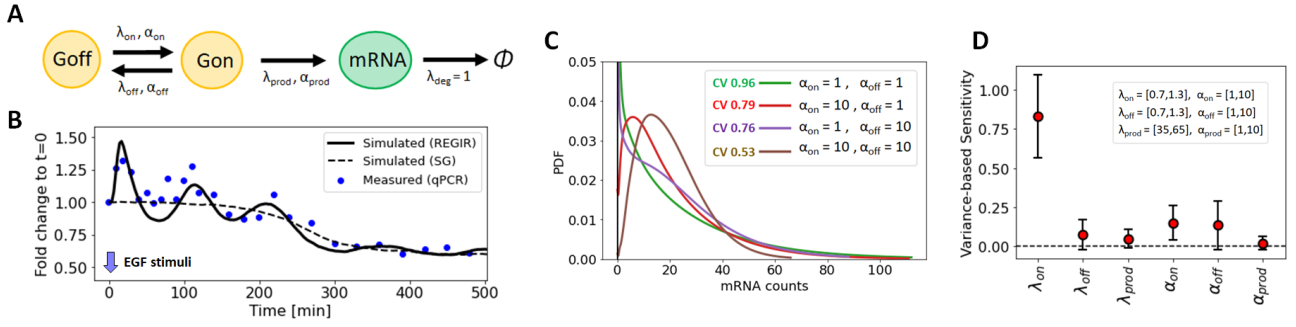


Figure 4: (A) Cartoon of the popular two-state model of RNA transcription, where the reactions obey non-Markovian stochastic dynamics. A gene promoter switches between an ON and an OFF state, and can produce an mRNA only when it is ON. The new mRNA degrades at a constant rate. (B) Average mRNA profile of the gene SLC7A5 after stimuli by epidermal growth factor (EGF) [58] measured by quantitative PCR (qPCR), where the mRNA count is normalized to be 1 at the instant of the stimuli. The simulated populations were averaged over 10k simulations and are provided for both the Markovian (SG, RMSD=0.016) and Non-Markovian model (REGIR, RMSD=0.0074), using for the latter the optimal parameter fit found with REGIR. (C) Steady-state density distribution of mRNA counts for different shape parameter combinations, where parameters $\lambda_{on} = 1$, $\lambda_{off} = 3$, $\lambda_{prod} = 100$ and $\alpha_{prod} = 1$ are kept fixed. Densities were estimated with a gaussian kernel after a log transformation (see methods). The corresponding coefficient of variation (CV) is indicated for each simulation. (D) Sobol variance-based sensitivity analysis of the CV of the steady-state single-cell mRNA distribution generated by the two-state model, with a grid of 128 points per parameter. λ_{on} , the parameter associated with the probability of a promoter being ON, has the highest influence on mRNA variance.

reveal the parameters relative to mRNA production (λ_{prod} , α_{prod}) to be the least sensitive. This is expected, as it has been shown analytically that the shape of the steady-state mRNA distribution is relatively insensitive to these provided that $\lambda_{prod} \gg \lambda_{on,off}$ [54, 35]. Interestingly, while there is a strong asymmetry between the sensitivities of rates λ_{on} and λ_{off} , the shape parameters α_{on} and α_{off} seems to affect equally the CV of the mRNA distribution. Additional insights can be obtained through the computation of phase diagrams [54, 56] (SI, Figure S9), where the impact of variation in the parameters can be assessed visually. We observe that, although sensitive, changing the shape parameters (α_{on} , α_{off}) do not affect significantly the phase diagrams of the CV, but rather approximately lower all CV values by a constant factor.

These results illustrate REGIR's capabilities to simulate both Markovian and non-Markovian dynamics under a wide range of RNA kinetics parameters, which can span several orders of magnitudes [55].

Rejection sampling allows for arbitrary approximation accuracy. In this section, we discuss the differences between nMGA [36] and REGIR in terms of simulation accuracy. We recall that both REGIR and nMGA are exact only when $\Delta t \rightarrow 0$, as they use a first-order Taylor approximation of the survival distribution function (SI, Section 2B). Indeed, the survival distribution function can be Taylor approximated as follows:

$$\Psi_j(\Delta t + t_j) = \Psi_j(t_j) - \psi_j(t_j) \Delta t + O(\psi_j'(t_j) \Delta t^2). \quad [9]$$

The approximation breaks down when the inequality $\psi_j(t_j) \gg \psi_j'(t_j) \Delta t$ is no longer verified.

The main difference between REGIR and nMGA lies in the introduction of the rejection step. In nMGA, the time increment until the next event is computed as:

$$\Delta t \text{ (nMGA)} = \frac{\ln(1/u)}{\sum_{j=1}^N \lambda_j(t_j)}, \quad [10]$$

while in REGIR, the expression becomes:

$$\Delta t \text{ (REGIR)} = \frac{\ln(1/u)}{N \cdot \lambda_{max}}. \quad [11]$$

From Eq. 10, it is clear that low rates are associated with large time increments Δt , and that in such a regime, the linear approximation nMGA used to compute Δt might fail (Eq. 9). Indeed, nMGA is only exact in the limit of an infinite number of reactants ($N \rightarrow \infty$) where it can be assumed that $\sum_{j=1}^N \lambda_j(t_j) \rightarrow \infty$. For processes characterized by low rates at some time points (such as gamma distribution at $t = 0$ for $\alpha > 1$), this approximation can be poor even in the limit of a large number of reactants. REGIR circumvents this problem by setting λ_{max} to an arbitrary large value (for example $\lambda_{max} \geq \lambda_0$), such that the time increment Δt remains *small enough* for the first order Taylor approximation (Eq. 9) to hold during the entire simulation. Still, this condition may not be sufficient when the number of processes N is too low (Figure 5A). For these cases, we introduce a new parameter f defined by the user, and set λ_{max} at each iteration such that:

$$\lambda_{max} \geq f \cdot \frac{\lambda_0}{N}. \quad [12]$$

The parameter f is chosen to guarantee a desired upper bound for Δt , e.g. such as $\psi_j(t_j) \gg \psi_j'(t_j) \Delta t$ always holds:

$$\Delta t \text{ (REGIR)} \leq \frac{\ln(1/u)}{f \cdot \lambda_0}. \quad [13]$$

Let us consider one reaction channel with N reactants following the toy reaction $A \rightarrow \emptyset$ (protein degradation), where the theoretical inter-event time distribution is equal to the distribution of times between two consecutive degradation events. This simple choice allows for the quantification of REGIR accuracy through the comparison between the theoretical and simulated REGIR inter-event time distributions. To quantify the change in accuracy as f increases, we compute the non-Markovian approximation error in terms of the earth mover distance (EMD) between the theoretical and simulated distributions (Figure 5B). Briefly, EMD reflects the minimal amount of *work* necessary to transform one distribution into another, where an EMD close to 0 indicates that distributions are nearly identical. We note that computing EMD scores requires randomly sampling both distributions, and therefore, even identical distributions will get a non-zero

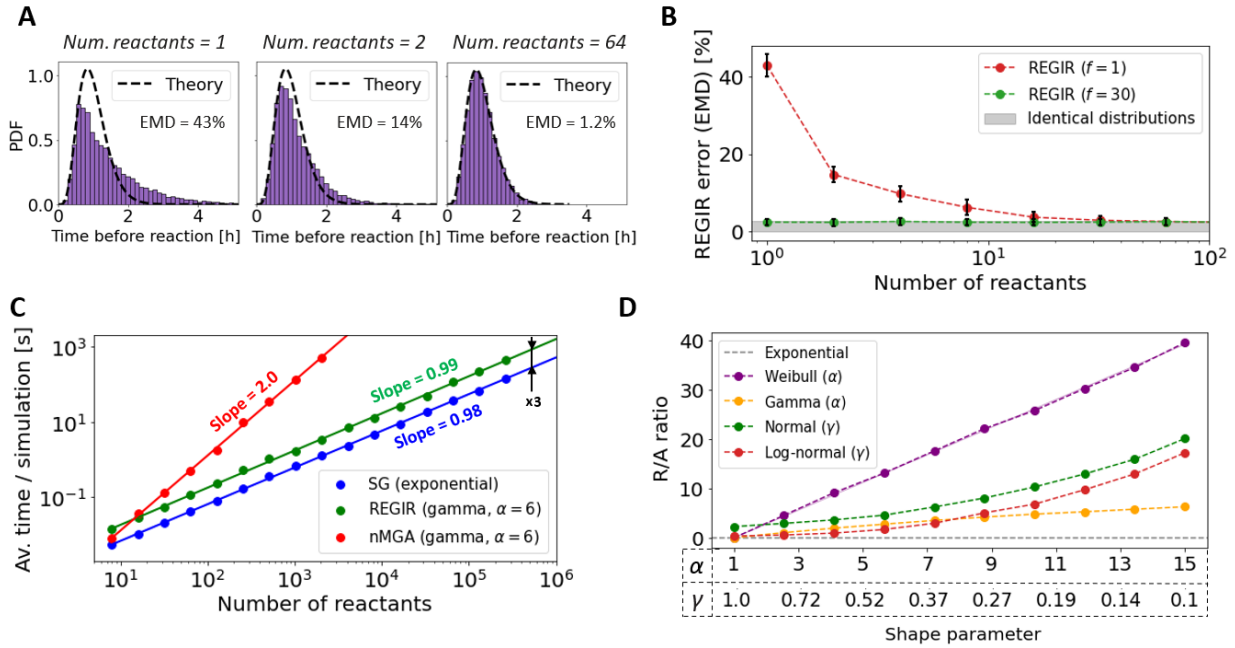


Figure 5: (A) REGIR approximation accuracy on a toy reaction $A \rightarrow \emptyset$ with a gamma inter-event distribution of shape parameter 6, visualized for different population sizes. The accuracy is computed using the earth mover distance (EMD) between the theoretical and simulated distributions, given in units of the distribution mean $1/\lambda_0$. In (B), we show how the EMD scales with the population size for two variations of REGIR, where the difference between the two lies in the additional parameter f used to define λ_{\max} . (C) Comparison of the computational time complexity of Markovian simulations (SG), and non-Markovian simulations run with REGIR and nMGA [36]. The benchmarking is performed on a toy $A \rightarrow A$ reaction with different numbers of reactants for a duration of $10/\lambda_0$, where $1/\lambda_0$ is the average inter-event time. Run times are averaged over 100 runs and slopes are obtained with a linear fit. A standard deviation of $\sim \pm 7\%$ was observed for all measurements. REGIR, while simulating non-Markovian processes, has an average runtime scaling linearly with the population size and only 3 times higher than SG. (D) Rejected over accepted reaction ratio (R/A) for different shape parameters of different distributions, averaged over 100 simulations, a standard deviation of $\sim \pm 12\%$ was observed for all measurements. Note that a direct comparison of the ratio across distributions is not meaningful as they have different standard deviations. We also note that R/A is scale-invariant and thus is independent of the distribution mean $1/\lambda_0$.

EMD, which we refer to as the EMD baseline. This comes from the fact that sampled points from equivalent distributions are not strictly equal, which results in an EMD on the order of 1% in our setup (SI, Section 6A). Fig. 5B shows the mean and standard deviation of EMD after repeating the sampling experiments 10 000 times for our toy example (gray area).

In our toy example $A \rightarrow \emptyset$, $f = 1$ yields an EMD score significantly above the baseline for $N < 30$ (Figure 5B), and thus, this is not a good parameter choice for low number of reactants. On the other hand, $f = 30$ results in EMD scores converging to the EMD baseline for all population sizes, thus validating this parameter choice in this toy example.

In general, f needs to be optimized for each system and dataset. Higher values of f lead to higher accuracy, but also to longer running times. A general recommendation is to keep f as low as compatible with a desired target accuracy given the number of reactants. Throughout this work, we have used $f = 30$, as this was the lowest value for which we could reach the EMD baseline regardless of the number of reactants (SI, Section 6B).

Importantly, the appropriate choice of f depends on the definition of the EMD baseline. Here, we define it by comparing distributions with 10k sampled points which yields a EMD baseline of $\sim 1\%$. This is reasonable as the best distribution fit we obtained in this work was 1.1%, achieved using a log-normal distribution to represent *Bacillus subtilis* inter-division distribution. The EMD baseline can be reduced

by increasing the number of sampled points, e.g. 100k samplings results in an EMD baseline of 0.2% (SI, Figure S10). Converging to this baseline would require $f = 200$, thus resulting in a 10-fold increase of the computational cost (SI, Section 6B).

Rejection sampling reduces the computational complexity from $O(N^2)$ to $O(N)$. We now consider one reaction channel with N reactants, following the toy reaction $A \rightarrow A$, which has the particularity of keeping the number of reactants constant throughout the entire simulation. Our results show that the simulation's runtime scales as $O(N)$ for both the SG and REGIR, while nMGA [36] scales as $O(N^2)$ (Figure 5C). Thus, the rejection step used by REGIR results in a significant simulation speed-up. To analyze theoretically the computational complexity of our algorithm, let us examine two different aspects of the simulation: (i) the computational complexity of a single time step and its scaling properties, and (ii) the number of steps required to simulate a fixed interval of length (T_{end}).

Let us first focus on the scaling properties of a single-time step. During a large simulation, two factors contribute to its computational cost, the calculation of the time step to the next reaction, and the update of the reactant populations [61]. For SG with one reaction channel, both of these steps are $O(1)$. In the case of nMGA however, these processes carry a computational cost of $O(N)$, as each reactant has its own reaction rate, which is equivalent to having its own

reaction channel. In particular, the update of the instantaneous rates can be very expensive, as it requires recalculating them for each process in the entire population after every simulation iteration. REGIR reduces the computational complexity to $O(1)$ using a rejection base approach, where only the rate of the drawn reactant is computed at each step. The maximum rate λ_{\max} is either kept constant throughout the simulation or is updated using an ordered data structure for storing the t_j values, thus also $O(1)$ (See Methods Section).

Regarding the number of steps required to simulate a fixed interval, both SG and nMGA scale linearly with the number of reactants N , because the time step becomes increasingly smaller as more channels are added to the simulation (Eq.2). The rejection approach of REGIR results in a larger number of time steps required to simulate a T_{end} interval, as a fraction of the time steps are rejected by the algorithm. The complexity then becomes $O(N) + O(R)$, where R refers to the number of rejected steps. From Eq.3 and Eq.4, we can compute the probability of rejection for a given iteration as:

$$\begin{aligned} p_{\text{reject}} &= 1 - p_{\text{accept}} \\ &= 1 - \frac{\sum_{j=1}^N p_j \lambda_j(t_j)}{\lambda_{\max}} \\ &= 1 - \frac{1}{N \lambda_{\max}} \sum_{j=1}^N \lambda_j(t_j) \\ &= 1 - \frac{\hat{\lambda}}{\lambda_{\max}}, \end{aligned} \quad [14]$$

where we have introduced $\hat{\lambda}$, the average rate. Then, the expected number of rejections before the first accepted reaction (A) is given by the mean of the geometric distribution with success probability p_{accept} :

$$\frac{R}{A} = \frac{1}{p_{\text{accept}}} - 1 = \frac{(\lambda_{\max} - \hat{\lambda})}{\hat{\lambda}} \quad [15]$$

Thus we can conclude that the scaling of the SG and REGIR running times, $T_{R, \text{SG}}$ and $T_{R, \text{REGIR}}$, are proportional according to the relation:

$$\frac{T_{R, \text{REGIR}}}{T_{R, \text{SG}}} = \frac{A + R}{A} = \frac{\lambda_{\max}}{\hat{\lambda}} \quad [16]$$

Indeed, from Figure 5C, we can compare the different scaling of the SG and REGIR running times. We notice that they are proportional by a factor of 3 for a gamma distribution of shape parameter 6, where we have assumed that both curves have a similar slope ~ 1 . Figure 5D shows the rejected over accepted reactions ratio (R/A) for various distribution and shape parameters. We note that the ratio significantly varies with the choice of distribution and the parameters. For instance, an exponential distribution has a ratio of 0 (since $\hat{\lambda} = \lambda_{\max} = \lambda_i \forall i$, no reaction is rejected). On the other side of the spectrum, the Weibull instantaneous rate increases polynomially with time (SI, Section 2), so the maximum rate λ_{\max} increases quickly with α , thus increasing the number of rejections. Other longer-tailed distributions with reaction rates increasing sub-linearly with time, e.g. the gamma distribution, will be less affected by changes in their respective shape parameter (Figure 5D, SI Section 2). In general, simulating a distribution with smaller variance will increase the maximum rate and as a result also increase the computational cost. This is intuitively clear from Figure 5D, where the rejected over accepted reaction ratio (R/A) monotonically increases with the shape parameter of the gamma

and Weibull distributions, which inversely correlate to the variance of their respective distribution. On the other hand, as both R and A are proportional to the rate λ_0 , the ratio R/A is independent of the mean inter-event time distribution $1/\lambda_0$ and thus scale invariant.

REGIR implementation. REGIR is implemented as a python library (`-pip install REGIR`), and its source code is accessible at <https://github.com/Aurelien-Pelissier/REGIR>. In addition to simulating non-Markovian processes, the library also allows users to perform sensitivity analysis and compute phase diagrams for their models. As the Systems Biology Markup Language (SBML) [62] is a standard for representing computational models in systems biology such as in the BioModels database [63], we adapt REGIR to this framework, where users can load and save their non-Markovian models in the SBML format.

Discussion. Non-Markovian stochastic systems are prevalent in many systems, especially in biological and cellular processes, where non-exponential waiting times, hidden states, feedback loops and time delays between reaction events usually result in the system exhibiting memory. A correct description is notoriously difficult and requires the use of non-Markovian analytical or simulation frameworks. At the analytical level, generalizations of the classical chemical master equation allowing for non-exponential waiting time distributions have been developed [64, 65]. While, in principle, its solution yields the probability density vector of the system at any time point, in practice, these equations can only be solved analytically in the simplest cases, and their numerical investigation is computationally expensive or even infeasible as the number of reachable states becomes large or even infinite. At the stochastic simulation level, non-Markovian frameworks suffer from similar challenges, and require strong simplifying assumptions, such as modeling inter-event times with a mixture of exponentials [37] or with exponential variables whose rates are allowed to change with time [36], to become computationally feasible. Even under these assumptions, these frameworks remain computationally expensive to run. Because of these complexities, most stochastic systems are analyzed using the Markovian assumption, which assumes that the system is memoryless, although this is far from being an accurate description of many cellular systems. Some generalizations have been proposed, such as Hidden Markov Models, which increase modeling flexibility by introducing hidden intermediate states, although this comes at the cost of a much larger number of parameters resulting in harder inference tasks.

Here we have introduced REGIR, a practical and scalable algorithm to efficiently simulate complex non-Markovian stochastic systems. REGIR enables the flexible and accurate modeling of stochastic processes where inter-event time distributions obey the most commonly used distributions, such as the exponential, gamma, normal, log-normal, and Weibull distributions. REGIR can simulate complex systems with many different reaction channels, while keeping a low computational cost via a rejection sampling approach. Concretely, rejection sampling enabled us to (i) reduce the computational complexity of non-Markovian frameworks from $O(N^2)$ (as in the nMGA [36]) to $O(N)$, thus reaching the same asymptotic complexity of the original Gillespie algorithm, and (ii) achieve an arbitrary user-define accuracy by introducing ad-

ditional rejections that further reduce the time step Δt (and therefore, the approximation error). As in all simulation frameworks, there is a trade-off between accuracy and running time. To control for this trade-off, REGIR introduces an additional parameter that enables a user to select a fixed accuracy, while maintaining the complexity at similar levels as Markovian algorithms such as the Gillespie algorithm.

We have demonstrated REGIR's capabilities in three different examples, namely, bacterial cell division, stem cell differentiation, and RNA transcription. Firstly, REGIR predicted the transient oscillations of *Caulobacter crescentus* populations that are expected according to deterministic models but lost when the system is simulated as a Markov model. Similarly, it recapitulated the dynamics of stem cell differentiation and accurately reproduced experimental data with a simple non-Markovian model that only required four parameters. Finally, we used REGIR to simulate mRNA transcription and replicated experimentally observed transient oscillations in mRNA levels that could not be produced with the Gillespie algorithm.

These examples demonstrate that REGIR enables the efficient simulation of complex non-Markovian systems and the investigation of how the distribution of inter-event times influences population dynamics. As this distribution is typically difficult to obtain experimentally, REGIR helps investigate the properties of the stochastic processes that drive the system dynamics. Furthermore, as REGIR describes the inter-event time distribution with two parameters – the rate λ_0 and the shape parameter α , it offers more flexibility to fit realistic population dynamics than Markovian models, which only admit one parameter per reaction channel. REGIR can infer the value of the distribution parameters directly from the data, and it can perform a Sobol variance-based sensitivity analysis to quantify the system's sensitivity to arbitrary perturbations of these parameters. It also enables the computation and visualization of phase diagrams depicting the changes in the mean, coefficient of variation, and entropy associated with changes in these parameters.

Nevertheless, all stochastic simulation frameworks can be slow when analyzing systems with a very high number of reactants and reaction channels. In such situations, viable options include using analytical simplifications to reduce the computational time, or running a few stochastic simulations, and training a neural network to perform a much larger number of simulations [66]. More importantly, both Markovian and non-Markovian frameworks struggle to efficiently simulate systems where the reaction propensities span several orders of magnitudes. In this regime, the vast majority of the time steps execute the reactions with the highest propensities, while reactions with lower propensities only occur rarely. This can result in a massive amount of computational time needed to reach steady-state, as has been observed in the numerical analysis of RNA transcription [67]. Piecewise-deterministic Markov process (PDMP) models provide a viable alternative, where low-frequency events are modeled with the Gillespie algorithm while high-frequency events are modeled by locally solving a system of ordinary differential equations. PDMP approaches were shown to considerably speed up simulations in several applications [67, 68, 69].

Finally, the rejection sampling approach implemented in REGIR allows for very high customization of both stochastic models and simulations. Since each reactant in the population can follow its own stochastic process, it is possible to tag each reactant with *individual properties*, such that its

reaction rate changes continuously according to external variables or functions. This possibility was exploited to model the birth and maturation of B cells, where each B cell was endowed with an individual B cell receptor that reacted differently to external cues [13, 14]. This modeling flexibility opens the exciting possibility of designing computationally efficient hybrid simulations, where the internal dynamics underlying each process are coupled to macro-population stochastic dynamics. In biochemistry, this approach can be used to simulate stochastic interactions between a high number of cells while maintaining the individual cell *identity* (i.e., DNA sequence, mRNA expression) [14, 16]. Although this article focused on biochemical applications, other research areas can greatly benefit from such stochastic simulation frameworks, such as finance, epidemiology, and information propagation in human networks. Indeed, hybrid models can better capture the internal complexity and diversity of individuals, and avoid relying on large-scale simulations based on overly simplistic assumptions [70].

To conclude, we described in this article a simple yet powerful framework that can simulate complex non-Markovian stochastic systems, with the hope that it becomes a new benchmark for the study of stochastic dynamic systems in various applications, including models from the BioModels database [63].

Materials and Methods

Code availability. The REGIR implementation, along with the data and the code to reproduce all figures presented in this article, is publicly available on Github at <https://github.com/Aurelien-Pelissier/REGIR>. The repository contains additional information regarding the REGIR interface with SBML models.

REGIR implementation optimization. The implementation focuses on two aspects to reduce significantly the computational cost of the algorithm. The first one is about the time since the last reaction of each process occurred (t_j). Rather than updating all of them at each time step, we only keep track of the timestamp the last reaction occurred t_{0j} , and then obtain t_j when needed as $t_j = t - t_{0j}$. The second one avoids the computation of λ_{\max} at each time step. Let us consider four possible scenarios:

- For distributions with a bounded instantaneous rate, such as the Cauchy or delayed exponential distribution, λ_{\max} can be kept constant as the upper bound.
- For unbounded distributions with a rate increasing monotonically with time, such as normal, Weibull ($\alpha > 1$) or gamma ($\alpha > 1$), the maximum rate is known by keeping track of the reactant that did not react for the longest time. $\lambda_{\max} = \lambda(t_{\max})$. As such, the maximum rate does not need to be updated until that reactant with maximum waiting time did not react.
- For unbounded distributions with a rate decreasing monotonically with time, such as Weibull ($\alpha < 1$), gamma ($\alpha < 1$) or power laws, the maximum rate is known by keeping track of the reactant that did not react for the shortest time. As this can result in a very large maximum rate in some situation, we do not recommend using REGIR for these long-tailed distributions, since they can be simulated more efficiently with the Laplace Gillespie algorithm [37].

- For distributions with arbitrary rates, such as the ones obtained numerically from experimental data, the user should precompute some bounds on $\lambda(t)$ for specific intervals, such that it can falls back to one of the three cases described above for each interval.

Earth mover distance. Also known as the Wasserstein or Kantorovich metric [71], the Earth mover distance (EMD) [46] is a measure of the distance between two probability distributions $P = [p_i]$ and $Q = [q_j]$ (i, j : index of instances in the probability distribution) over a metric space D . Where $D = [d_{i,j}]$ is the ground distance between clusters $[p_i]$ and $[q_j]$. EMD reflects the minimal amount of *work* that must be used to transform one distribution into the other by moving *distribution mass* around. To compute EMD, we first need to find the optimal flow $F = [f_{i,j}]$ to minimize the overall cost when moving from P to Q.

$$\min \sum_{i=1}^n \sum_{j=1}^m f_{i,j} d_{i,j} \quad [17]$$

Finding the optimal flow F is typically related to an instance of the transportation problem, and can be efficiently solved in polynomial time [72]. EMD is then defined as the minimal work normalized by the total flow:

$$\text{EMD}(P, Q) = \frac{\sum_{i=1}^n \sum_{j=1}^m f_{i,j} d_{i,j}}{\sum_{i=1}^n \sum_{j=1}^m f_{i,j}} \quad [18]$$

Note that EMD satisfies the metric properties, i.e., positivity, symmetricity, triangle inequality, and free from any choice of bin size if $d_{i,j}$ follows the metric properties

In our application, the EMD between inter-event time distribution is quantified in unit of time. However, to ensure consistency of the EMD value over different parameter space, we normalize the distance matrix $[d_{i,j}]$ by the mean inter event time ($1/\lambda_0$) of the reaction channel. We use the Fast EMD python implementation [73] to efficiently compute the distances. The distances are measured by sampling 1×10^4 points from both the theoretical and simulated inter-event distributions, which result in an intrinsic EMD on the order of 1% (Figure S10). This comes from the fact that sampled points from equivalent distributions will not be strictly equal, which will result in a non-zero EMD.

Parameter optimization. For each REGIR simulation, we quantify its *accuracy* by comparing the simulated population dynamics to the experimentally measured populations. We define the *score* of the model as the root mean square deviations (RMSD) between the measured and simulated population averaged over all timepoints and reactants. In the case of the stem cell differentiation, the populations describe proportions bounded between 0 and 1. This may bias the the optimization towards ignoring variations close to very low (~ 0) and very high (~ 1) values, as a proportion of 98% will be considered closer to 99% than 50% is to 52%. To correct for this bias, we transform both simulated and measured populations with an inverse sigmoid function. For experimental reasons, proportions lower than 1% or higher than 99% are considered not reliable enough, so we only apply the transformation within that range:

$$\begin{aligned} y_{\text{new}} &= \log\left(\frac{y}{1-y}\right) \quad \text{for } 1\% \leq y \leq 99\% \\ y_{\text{new}} &= 4.6 \quad \text{for } y > 99\% \\ y_{\text{new}} &= -4.6 \quad \text{for } y < 1\% \end{aligned} \quad [19]$$

Then, the score function is minimized with the maxLIP0 algorithm [74], which is both parameter free and provably better than a random search. It is a good alternative to Bayesian optimization methods [75], that typically require the definition of prior assumptions about the function being optimized and thus require domain knowledge.

Density estimation of mRNA distribution. Generally, considering a kernel density estimator for a random variable $Y = g(X)$ denoted $f_Y(y)$, one can retrieve the density function of X , denoted $f_X(x)$, with the relation (up to a scaling factor) [76]

$$f_X(x) \sim f_Y(y) \left| \frac{d}{dx} g(x) \right|. \quad [20]$$

Since in our problem, the mRNA density count is bounded between $[0, +\infty]$, we cannot estimate the density directly with a gaussian kernel as it may infer non zero density for negative mRNA counts. Thus, we first transform mRNA counts with the function $y = g(x) = \log(x)$ so that the transformed data is unbounded ($[-\infty, +\infty]$). Then, we retrieve the density of the mRNA counts with

$$f_X(x) \sim \frac{f_Y(\log(x))}{x}.$$

Variance-based sensitivity analysis. A variance-based sensitivity analysis decomposes the variance of the output of the model $\text{Var}(Y)$ into fractions which can be attributed to inputs $\{S_i\}$, where a first order sensitivity index is defined as

$$S_i = \frac{V_i}{\text{Var}(Y)},$$

We note that with this definition, the sum of the sensitivities over all input parameters is always one ($\sum S_i = 1$). We estimate sensitivity indices numerically with a quasi-Monte Carlo method, where points are sampled with the Sobol quasi-random sequences [60]. The python library `Salib` [77] is used to perform this analysis.

Acknowledgements. The authors thank Jonathan Karr, Farshid Jafarpour, Srividya Iyer-Biswas and Peter Ashcroft for their valuable suggestions. This research was supported by the COSMIC European Training Network, funded from the European Union's Horizon 2020 research and innovation program under grant agreement No 765158.

A Probability density functions and instantaneous rates in the REGIR framework

A.1 Parametrization of inter-event time distributions

For consistency with other works in the literature of stochastic simulations, we parameterize processes using their mean $\frac{1}{\lambda_0}$, where λ_0 would be the instantaneous rate if the distribution was exponential. Additionally, some distributions require a second parameter to describe their *shape*. For the normal and log-normal distribution, we use γ , a scale free standard deviation defined as the standard deviation over the mean. For the gamma and Weibull distributions we use α , the shape parameter in their standard parametrization. Thus, all inter-event time distributions in this article are parametrized with two variables, (λ_0, α) or (λ_0, γ) .

Normal distribution. The normal distribution is typically parametrized by the mean μ and the standard deviation σ , as follows:

$$\text{normal}(t; \mu, \sigma) = \frac{1}{\sigma\sqrt{2\pi}} \exp\left(-\frac{1}{2}\left(\frac{t-\mu}{\sigma}\right)^2\right). \quad [21]$$

The parameters μ and σ can be chosen such as the mean inter event time distribution $1/\lambda_0$ with:

$$\mu = \frac{1}{\lambda_0} \text{ and } \sigma = \frac{\gamma}{\lambda_0}$$

Where γ corresponds to ratio between the standard deviation and the mean, representing a scale-free standard deviation. The alternative parametrization of the distribution for REGIR is then given by

$$\boxed{\text{normal}(t; \lambda_0, \gamma) = \frac{\lambda_0}{\gamma\sqrt{2\pi}} \exp\left(-\frac{1}{2}\left(\frac{\lambda_0 t - 1}{\gamma}\right)^2\right)}. \quad [22]$$

Log-normal distribution. The log-normal distribution is typically parametrized by μ and σ , as follows:

$$\text{log-normal}(t; \mu, \sigma) = \frac{1}{t\sigma\sqrt{2\pi}} \exp\left(-\frac{(\log(t) - \mu)^2}{2\sigma^2}\right), \quad [23]$$

The mean and variance are given by:

$$\begin{aligned} \text{mean} &= \exp\left(\mu + \frac{\sigma^2}{2}\right), \\ \text{variance} &= \left[\exp(\sigma^2) - 1\right] \exp(2\mu + \sigma^2). \end{aligned}$$

If we want the mean inter event time distribution to be $1/\lambda_0$, we chose μ and σ as follows:

$$\mu = \log\left(\frac{1}{\lambda_0\sqrt{1+\gamma^2}}\right) \text{ and } \sigma = \sqrt{\log(1+\gamma^2)}.$$

Where, as with the normal distribution, γ corresponds to the ratio between the standard deviation and the mean, and thus, it is scale invariant. The alternative parametrization of the distribution for REGIR is then given by

$$\boxed{\text{log-normal}(t; \lambda_0, \gamma) = \frac{1}{t\sqrt{2\pi}\log(1+\gamma^2)} \exp\left(-\frac{\left(\log(t) + \log(\lambda_0\sqrt{1+\gamma^2})\right)^2}{2\log(1+\gamma^2)}\right)}, \quad [24]$$

Gamma distribution. The gamma distribution admits 2 constants, α and β :

$$\text{gamma}(t; \alpha, \beta) = \frac{\beta^\alpha}{\Gamma(\alpha)} t^{\alpha-1} e^{-\beta t}. \quad [25]$$

Mean and variance can be computed to be:

$$\begin{aligned} \text{mean} &= \frac{\alpha}{\beta}, \\ \text{variance} &= \frac{\alpha}{\beta^2}. \end{aligned}$$

The parameter β can be chosen such as the mean inter event time distribution is $1/\lambda_0$:

$$\beta = \alpha \lambda_0.$$

Thus, we parametrize the gamma distribution as

$$\boxed{\text{gamma}(t; \lambda_0, \alpha) = \frac{(\alpha \lambda_0)^\alpha}{\Gamma(\alpha)} t^{\alpha-1} e^{-\alpha \lambda_0 t}.} \quad [26]$$

We note that in this case the ratio between the standard deviation and the mean is related the the shape parameter α with:

$$\gamma = \frac{1}{\sqrt{\alpha}},$$

Weibull distribution. The Weibull distribution [41] can be parametrized with constants λ and α as follows:

$$\text{Weibull}(t; \lambda, \alpha) = \frac{\alpha}{\lambda} \left(\frac{t}{\lambda} \right)^{\alpha-1} e^{-(t/\lambda)^\alpha}. \quad [27]$$

The mean and variance are:

$$\begin{aligned} \text{mean} &= \lambda \Gamma \left(1 + \frac{1}{\alpha} \right), \\ \text{variance} &= \lambda^2 \left[\Gamma \left(1 + \frac{2}{\alpha} \right) - \Gamma^2 \left(1 + \frac{1}{\alpha} \right) \right]. \end{aligned}$$

If t represents a "time-to-failure", the Weibull distribution gives a distribution for which the failure rate is proportional to a power of time. An alternative parametrisation often found in text books is $\lambda = \left(\frac{\alpha}{\beta} \right)^{\frac{1}{\alpha}}$, under which the PDF of the Weibull distribution becomes:

$$\text{Weibull}(t; \beta, \alpha) = \beta t^{\alpha-1} \times \exp \left(-\frac{\beta t^\alpha}{\alpha} \right). \quad [28]$$

To make the mean inter event time distribution equal to $1/\lambda_0$, β has to be chosen as follows:

$$\beta = (\alpha + 1) \left[\lambda_0 \Gamma \left(\frac{\alpha + 2}{\alpha + 1} \right) \right]^{\alpha+1}.$$

Thus, we parametrize the gamma distribution as

$$\boxed{\text{Weibull}(t; \lambda_0, \alpha) = (\alpha + 1) \left[\lambda_0 \Gamma \left(\frac{\alpha + 2}{\alpha + 1} \right) \right]^{\alpha+1} t^{\alpha-1} \times \exp \left(-\frac{(\alpha + 1) \left[\lambda_0 \Gamma \left(\frac{\alpha + 2}{\alpha + 1} \right) \right]^{\alpha+1} t^\alpha}{\alpha} \right).} \quad [29]$$

We note that with this choice, the ratio between the standard deviation and the mean is related to α with:

$$\gamma = \frac{\Gamma \left(\frac{\alpha+2}{\alpha} \right)}{\Gamma^2 \left(\frac{\alpha+1}{\alpha} \right)} - 1.$$

Cauchy distribution. The Cauchy distribution admits two parameters, μ and σ :

$$\text{Cauchy}(t; \mu, \sigma) = \frac{1}{\pi\sigma \left[1 + \left(\frac{t-\mu}{\sigma} \right)^2 \right]}. \quad [30]$$

The Cauchy distribution represents the distribution of the ratio of two independent and normally distributed random variables with mean zero. The mean and variance are undefined, as the integrals necessary to compute these values do not exist¹. Intuitively, this happens because extremely large number can be drawn with non-zero probability. Nevertheless, we can choose the parameter μ as the inverse of the median inter event time $1/\lambda_0$:

$$\mu = \frac{1}{\lambda_0}.$$

Similarly, we can define γ as the *analogue* of ratio between the standard deviation and the mean, which is scale invariant:

$$\sigma = \frac{\gamma}{\lambda_0}.$$

Thus, we parametrize the Cauchy distribution as

$$\boxed{\text{Cauchy}(t; \lambda_0, \gamma) = \frac{1}{\pi \frac{\gamma}{\lambda_0} \left[1 + \left(\frac{\lambda_0 t - 1}{\gamma} \right)^2 \right]}.} \quad [31]$$

A.2 Relationship between probability density functions and instantaneous rates

We consider the survival distribution function (SDF) $\Psi(t)$ of a renewal process:

$$\Psi(t) = \int_t^\infty \psi(\tau) d\tau \quad [32]$$

and its relationship with the probability distribution function (PDF) $\psi(t) = -\frac{d\Psi(t)}{dt}$. Using the definition of the instantaneous rate function:

$$\lambda(t) = \frac{\psi(t)}{\Psi(t)}, \quad [33]$$

we can describe the time evolution of $\Psi(t)$ as a first order homogeneous differential equation:

$$\lambda(t) \Psi(t) + \Psi'(t) = 0. \quad [34]$$

The general solution is easily written as [78]:

$$\Psi(t) = K \exp\left(-\int_0^t \lambda(\tau) d\tau\right), \quad [35]$$

where $K \in \mathbb{R}$ is an integration constant. However, since by definition $\Psi(0) = 1$, we conclude that $K = 1$. The PDF of that process can now be computed as follows:

$$\psi(t) = -\frac{d\Psi}{dt}(t) = \lambda(t) \exp\left(-\int_0^t \lambda(\tau) d\tau\right) \quad [36]$$

Note that $\Psi(t)$ verifies the additional normalization condition $\Psi(\infty) = 0$. This implies:

$$\begin{aligned} \Psi(\infty) &= \exp\left(-\int_0^\infty \lambda(\tau) d\tau\right) = 0 \\ \Rightarrow \int_0^\infty \lambda(\tau) d\tau &= \infty \end{aligned} \quad [37]$$

This means that $\lambda(t)$ has to be chosen such as its definite integral from 0 to ∞ is infinite, otherwise $\psi(t)$ and $\Psi(t)$ do not represent a renewal process.

¹The integral associated with the mean, $\int_{-\infty}^\infty xf(x) dx$, does not exist. This can be proven, for instance, by noticing that $\lim_{a \rightarrow \infty} \int_{-a}^a xf(x) dx$ and $\lim_{a \rightarrow \infty} \int_{-2a}^a xf(x) dx$ converge to different values. Similar arguments can be used to show that the variance does not exist either.

Examples

In general, the instantaneous rate for any distribution can be computed as $\lambda(t) = \frac{PDF(t)}{SDF(t)}$, where the survival distribution function (SDF) is related to the cumulative distribution function (CDF) according to $SDF = 1 - CDF$. We provide here a few examples of instantaneous rate functions and their associated PDFs:

- $\lambda(t) = a_0$ leads to $PDF = a_0 \times \exp(-a_0 t)$ and $SDF = \exp(-a_0 t)$, which represent an exponential distribution.
- $\lambda(t) = \beta t^{\alpha-1}$ leads to $PDF = \beta t^{\alpha-1} \times \exp\left(-\frac{\beta t^\alpha}{\alpha}\right)$ and $SDF = \exp\left(-\frac{\beta t^\alpha}{\alpha}\right)$, associated with the Weibull distribution [41].
- $\lambda(t) = \frac{c^2 t}{1 + ct}$ leads to $PDF = c^2 t \times \exp(-ct)$ and $SDF = (1 + ct) \times \exp(-ct)$.
- Many important distributions do not have a simple analytic form for the instantaneous rate. For instance, the normal distribution, $PDF = \frac{1}{\sigma\sqrt{2\pi}} e^{-\frac{1}{2}\left(\frac{t-\mu}{\sigma}\right)^2}$ and $SDF = \frac{1}{2} \left[1 - \text{erf}\left(\frac{t-\mu}{\sigma\sqrt{2}}\right)\right]$, with erf being the error function [79], results in an instantaneous rate that cannot be expressed in terms of basic functions. An approximation is however possible at large times, where the instantaneous rate asymptotically approximates a linear function $\lambda(t) \approx \frac{t-\mu}{\sigma^2}$.

In Figure 6B, we show that the normal, Weibull ($\alpha \geq 1$) and gamma ($\alpha \geq 1$) distributions have monotonically increasing rates, while the Cauchy and log-normal distributions exhibit a maximum.

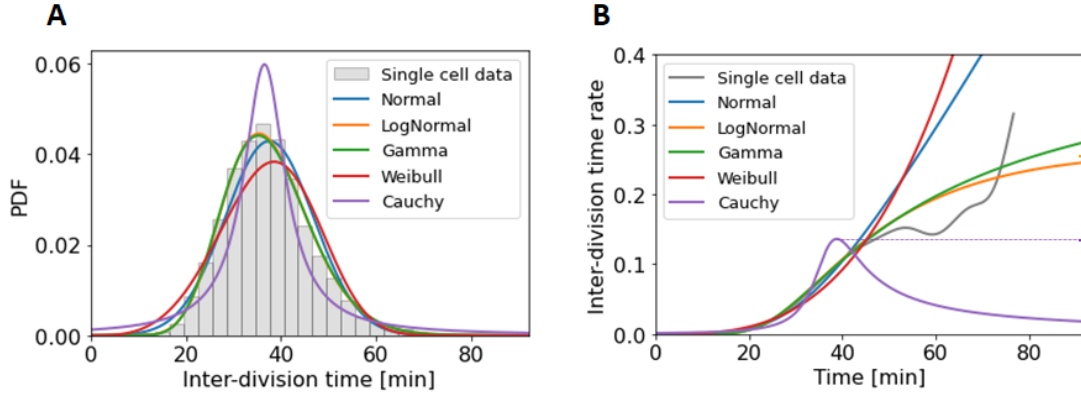


Figure 6: (A) PDF of several distributions typically used to represent biochemical waiting times, where the parameters have been chosen to fit the measured inter-division time of *Bacillus subtilis* [43] at constant temperature. (B) Although the PDFs are relatively similar, the instantaneous rates show markedly different behaviors as a function of time. The single cell instantaneous rate was estimated with a gaussian kernel density estimator. When finite, the maximum of instantaneous rates are displayed on the right of the figure.

B The Rejection Gillespie algorithm for non-Markovian Reactions

We consider N Poisson processes running in parallel, each with their respective reaction rate λ_j ($1 \leq j \leq N$), and denote by $a_0 = \sum \lambda_j$ the sum of the individual rates. The standard Gillespie (SG) algorithm is a popular stochastic simulation framework that can generate statistically correct trajectories of a stochastic equation system. The algorithm assumes that the reaction rates are known and constant, under which assumption, a trajectory can be obtained using the following iterative rules (see [37] for the full derivation):

- (i) Draw $u \in \mathcal{U}^{[0,1]}$ a random variate from the uniform density on the interval $[0, 1]$, and compute the time increment to the next event with

$$\Delta t = \frac{\ln(1/u)}{a_0}, \quad [38]$$

- (ii) Draw the process j that has produced the event with probability

$$P_j = \frac{\lambda_j}{a_0}, \quad [39]$$

In the main text, we introduced the Rejection Gillespie for non-Markovian Reactions (REGIR) that is statistically exact in the limit of $\Delta t \rightarrow 0$ (Equation 5 of the main text). Below, we provide the proof, which we decompose into two independent subpart. First, we show that the introduction of rejected steps in the Gillespie model is mathematically equivalent to the standard Gillespie (SG) algorithm. Second, we show that locally considering each process as Poissonian during the time step Δt at each Gillespie iteration yield statistically exact results for non-Markovian simulations when $\Delta t \rightarrow 0$. We note that both of these aspects were already proven separately in reference [39] and [36], respectively. Here we put them together for the reader's convenience. As the rejection framework allows for arbitrarily reduction of Δt by increasing λ_{\max} , REGIR is exact in the limit $\lambda_{\max} \rightarrow \infty$ or $N \rightarrow \infty$.

B.1 Proof for the Rejection based Gillespie Algorithm

The rejection based Gillespie algorithm will follow the same distribution as Standard Gillespie (SG) if and only if (iff):

- (i) The reaction R_j occurs with probability $P = \lambda_j/a_0$.
- (ii) The Δt increment in time follows the same exponential distribution as in SG, i.e. $f_{\Delta t}(x) = a_0 \cdot \exp(-a_0x)$.

(i) Reaction R_j accepted with the same probability as in SG

We define $p_{\text{accept}}(R_j)$ as the joint probability of R_j being first selected and then accepted, λ_{\max} as the upper propensity bound for all reactions, and $a_{0,\max} = N\lambda_{\max}$. We can write

$$p_{\text{accept}}(R_j) = \frac{\lambda_{\max}}{a_{0,\max}} \times \frac{\lambda_j}{\lambda_{\max}} = \frac{\lambda_j}{a_{0,\max}}$$

We then denote by $p_{\text{accept}}(R)$ the probability of any reaction being accepted:

$$p_{\text{accept}}(R) = \frac{a_0}{a_{0,\max}}.$$

The conditional probability $p_{\text{accept}}(R_j | R)$ can be exploited to show the probability of R_j being accepted given that some reaction had been accepted:

$$p_{\text{accept}}(R_j | R) = \frac{p_{\text{accept}}(R_j)}{p_{\text{accept}}(R)} = \left(\frac{\lambda_j}{a_{0,\max}} \right) / \left(\frac{a_0}{a_{0,\max}} \right) = \frac{\lambda_j}{a_0}$$

(ii) The time increment Δt follows an exponential PDF

We denote by k the number of trials until the reaction is accepted (thus $k - 1$ rejections until success), with time being advanced by increment of $\Delta t = -\ln(u)/a_{0,\max}$ after each attempt. It follows that for k attempts,

$$\Delta t = -\frac{1}{a_{0,\max}} \ln \left(\prod_{i=1}^k u_i \right) \quad [40]$$

which corresponds to an Erlang distribution with parameters k and $a_{0,\max}$ (represents the time elapsed until the k th event of a Poisson process with rate $a_{0,\max}$). In addition, k is geometrically distributed with probability $p_{\text{accept}}(R)$, i.e.

$$P(X = k) = (1 - p_{\text{accept}}(R))^{k-1} \times p_{\text{accept}}(R).$$

As the PDF for Δt can be expressed as the derivative of its CDF, we can write

$$\begin{aligned} f_{\Delta t}(x) &= \frac{d}{dx} F_{\Delta t}(x) \\ &= \frac{d}{dx} P(\Delta t \leq x), \end{aligned}$$

where $P(\Delta t \leq x)$ can be partitioned for values of k :

$$\begin{aligned} &= \frac{d}{dx} \sum_{k=1}^{\infty} P(\Delta t \leq x | X = k) P(X = k) \\ &= \frac{d}{dx} \sum_{k=1}^{\infty} P(\Delta t \leq x | X = k) \left(1 - \frac{a_0}{a_{0,\max}} \right)^{k-1} \frac{a_0}{a_{0,\max}} \end{aligned}$$

and as shown in equation 40, the distribution of Δt parametrized by k follows an Erlang distribution:

$$\begin{aligned}
 &= \sum_{k=1}^{\infty} \frac{d}{dx} F_{\text{Erlang}(k, \lambda_{0, \max})} \left(1 - \frac{a_0}{a_{0, \max}} \right)^{k-1} \frac{a_0}{a_{0, \max}} \\
 &= \sum_{k=1}^{\infty} f_{\text{Erlang}(k, \lambda_{0, \max})} \left(1 - \frac{a_0}{a_{0, \max}} \right)^{k-1} \frac{a_0}{a_{0, \max}} \\
 &= \sum_{k=1}^{\infty} \frac{a_{0, \max}^k \cdot x^{k-1} \cdot \exp(-a_{0, \max} x)}{(k-1)!} \cdot \left(\frac{a_{0, \max} - a_0}{a_{0, \max}} \right)^{k-1} \cdot \frac{a_0}{a_{0, \max}} \\
 &= a_0 \exp(-a_{0, \max} x) \sum_{k=1}^{\infty} \frac{(a_{0, \max} - a_0)^{k-1} \cdot x^{k-1}}{(k-1)!} \\
 &= a_0 \exp(-a_{0, \max} x) \cdot \exp(x \cdot (a_{0, \max} - a_0)) \\
 &= a_0 \cdot \exp(-a_0 x).
 \end{aligned}$$

Hence, in Rejection Gillespie, Δt follows the same exponential distribution as in the SG.

B.2 Proof for the Non Markovian Gillespie Algorithm (nMGA)

In this section, we summarize the proof given by Boguna [36], and consider a second order approximation of their algorithm. We consider N renewal processes running in parallel, and denote by t_j the time elapsed since the last event of the j th process ($1 \leq j \leq N$). We denote by $\psi_j(t_j)$ the probability density function of inter-event times for the j th process, and by

$$\Psi_j(t_j) = \int_{t_j}^{\infty} \psi_j(\tau) d\tau$$

the survival function of the j th process, i.e., the probability that the inter-event time is larger than t_j . We also set

$$\Phi(\Delta t | \{t_j\}) = \prod_{j=1}^N \frac{\Psi_j(t_j + \Delta t)}{\Psi_j(t_j)}$$

which is the probability that no process generates an event for time Δt [37]. Then in the non Markovian Gillespie algorithm (nMGA), the time until the next event, Δt , is computed by solving $\Phi(\Delta t | \{t_j\}) = u$, where $u \in \mathcal{U}^{[0,1]}$ is a random variate drawn from the uniform density on the interval $[0, 1]$. This can be time consuming for some distributions [36]. In the limit of large number of processes $N \rightarrow \infty$, we can simplify the numerical computation of the time Δt needed in the algorithm. We start by rewriting the function $\Phi(\Delta t | t_j)$ as:

$$\Phi(\Delta t | \{t_j\}) = \exp \left[- \sum_{j=1}^N \ln \left(\frac{\Psi_j(t_j)}{\Psi_j(\Delta t + t_j)} \right) \right] \quad [41]$$

The sum within the exponential function is a sum of N monotonously increasing functions of Δt . Therefore, when $N \rightarrow \infty$, the survival probability $\Phi(\Delta t | \{t_j\})$ is close to zero everywhere except when $\Delta t \sim 0$. Hence we only need to consider $\Phi(\Delta t | \{t_j\})$ around $\Delta t = 0$, where a Taylor expansion in small Δt can be performed: $\Psi_j(\Delta t + t_j) = \Psi_j(t_j) - \psi_j(t_j) \Delta t + O(\Delta t^2)$. Plugging this expression into Eq. 41, using the approximation $\ln(1+x) = x + O(x^2)$ and $1/(1-x) = 1+x + O(x^2)$ for $x \rightarrow 0$, we can write:

$$\begin{aligned}
 \Phi(\Delta t | \{t_j\}) &= \exp \left[- \sum_{j=1}^N \ln \frac{\Psi_j(t_j)}{\Psi_j(t_j) - \psi_j(t_j) \Delta t + O(\Delta t^2)} \right] \\
 &= \exp \left[- \sum_{j=1}^N \ln \frac{\Psi_j(t_j)}{\Psi_j(t_j) - \psi_j(t_j) \Delta t + O(\Delta t^2)} \right] \\
 &\approx \exp \left[- \Delta t \left(\sum_{j=1}^N \lambda_j(t_j) \right) \right]
 \end{aligned} \quad [42]$$

Where the instantaneous rate λ_j is defined as:

$$\lambda_j(t_j) = \frac{\psi_j(t_j)}{\Psi_j(t_j)}.$$

With this approximation, the time until the next event is determined by

$$\Phi(\Delta t | \{t_j\}) \approx \exp \left[-\Delta t \left(\sum_{j=1}^N \lambda_j(t_j) \right) \right] = u, \quad [43]$$

i.e.,

$$\Delta t = \frac{\ln(1/u)}{\sum_{j=1}^N \lambda_j(t_j)}. \quad [44]$$

This means that Δt is exponentially distributed, and indicates that nMGA is locally considering each process as Poissonian during the time step Δt . We note that by eliminating the time dependency of $\lambda_j(t_j)$, i.e. by setting $\lambda_j(t_j) = \lambda_j$, we recover the SG algorithm.

Second-order approximation

We can also consider a quadratic expansion of Eq. 41, which results in a second-order approximation of the time interval Δt . In order to do so, we first expand up to second order $\Psi_j(\Delta t + t_j)$:

$$\Psi_j(\Delta t + t_j) = \Psi_j(t_j) - \psi_j(t_j) \Delta t - \psi'_j(t_j) \Delta t^2 / 2 + O(\Delta t^3). \quad [45]$$

Additionally, the instantaneous rate $\lambda_j = \psi_j / \Psi_j$ is related to its derivative λ'_j through the relation (we remind that $\Psi'_j = -\psi_j$):

$$\lambda'_j = \left(\frac{\psi_j}{\Psi_j} \right)' = \frac{\psi'_j \Psi_j - \psi_j \Psi'_j}{\Psi_j^2} = \frac{\psi'_j}{\Psi_j} + \left(\frac{\psi_j}{\Psi_j} \right)^2 = \frac{\psi'_j}{\Psi_j} + \lambda_j^2. \quad [46]$$

Plugging this expression into Eq. 41, using the approximation $1/(1-x) = 1+x+x^2+O(x^3)$ and $\ln(1+x) = x - x^2/2 + O(x^3)$ for $x \rightarrow 0$, we obtain:

$$\begin{aligned} \Phi(\Delta t | \{t_j\}) &= \exp \left[-\sum_{j=1}^N \ln \frac{1}{1 - \lambda_j(t_j) \Delta t - \left(\lambda'_j(t_j) - \lambda_j^2(t_j) \right) \frac{\Delta t^2}{2} + O(\Delta t^3)} \right] \\ &= \exp \left[-\sum_{j=1}^N \ln \left(1 + \lambda_j(t_j) \Delta t + \left(\lambda'_j(t_j) + \lambda_j^2(t_j) \right) \frac{\Delta t^2}{2} + O(\Delta t^3) \right) \right] \\ &= \exp \left[-\sum_{j=1}^N \left(\lambda_j(t_j) \Delta t + \lambda'_j(t_j) \frac{\Delta t^2}{2} + O(\Delta t^3) \right) \right] \end{aligned}$$

Solving $\Phi(\Delta t | \{t_j\}) = u$ to determine the next time increment Δt , we get a quadratic equation for which we take the positive solution:

$$\Delta t = \frac{-\sum_{j=1}^N \lambda_j(t_j) + \sqrt{\left(\sum_{j=1}^N \lambda_j(t_j) \right)^2 + 2 \left(\sum_{j=1}^N \lambda'_j(t_j) \right) \cdot \ln(1/u)}}{\left(\sum_{j=1}^N \lambda'_j(t_j) \right)} \quad [47]$$

Interestingly, Δt is no longer exponentially distributed and thus the rejection framework described in the first part cannot be applied with the second order approximation of nMGA.

C Non-Markovian division

C.1 Symmetric division

A simple system following non-Markovian dynamics that can be described analytically is symmetric division, where a single type of reactant A reacts to produce $\nu > 1$ identical versions of itself. We thus consider the reaction $A \rightarrow \nu A$. In the general case, the population's steady state exponential growth rate k is related to the single-cell division time distribution $\psi(t)$ through the integral [48]

$$\mathcal{L}\{\psi\}(k) = \int_0^\infty e^{-k\tau} \psi(\tau) d\tau = \frac{1}{\nu}. \quad [48]$$

In words, k is the point at which the Laplace transform of the division time distribution $\psi(\tau)$ is equal to $1/\nu$. Then, the mean doubling time of the population is obtained with $t_2 = \ln(2)/k$. Defining the mean division time of single cells as $\mu = \int_0^\infty t\psi(t)dt$, we can solve the above equation for particular cases.

Deterministic processes. For a deterministic division (Dirac distribution), with PDF $\psi(t) = \delta(t - \mu)$, the Laplace transform is given by

$$\mathcal{L}\{\psi\}(k) = \exp(-\mu k). \quad [49]$$

Thus, we can simplify equation 48 into

$$\exp\left(-\frac{\ln(2) \cdot \mu}{t_2}\right) = \frac{1}{\nu} \text{ which yields } t_2 = \mu \cdot \frac{\ln(2)}{\ln(\nu)}. \quad [50]$$

Markovian processes. For an exponential distribution, with PDF $\psi(t) = \lambda e^{-\lambda t}$, the Laplace transform is given by

$$\mathcal{L}\{\psi\}(k) = \frac{\lambda}{k + \lambda}. \quad [51]$$

Replacing $\lambda = 1/\mu$, we can simplify equation 48 into

$$\frac{1}{1 + \mu \ln(2)/t_2} = \frac{1}{\nu} \text{ which yields } t_2 = \mu \cdot \frac{\ln(2)}{\nu - 1}. \quad [52]$$

Non-Markovian processes. From Eq.48, the population doubling time can be computed exactly for any distributions with an analytical form of its Laplace transform. We provide an example with the gamma distribution, with PDF $\psi(t) = \frac{\beta^\alpha}{\Gamma(\alpha)} t^{\alpha-1} e^{-\beta t}$ and Laplace transform

$$\mathcal{L}\{\psi\}(k) = \frac{\beta^\alpha}{(\beta + k)^\alpha}. \quad [53]$$

Replacing $\beta = \alpha/\mu$, we can simplify equation 48 into

$$\frac{1}{1 + \mu \ln(2)/(\alpha t_2)} = \left(\frac{1}{\nu}\right)^{1/\alpha} \text{ which yields } t_2 = \mu \cdot \frac{\ln(2)}{\alpha (\nu^{1/\alpha} - 1)} \quad [54]$$

where $\alpha = 1$ recovers the Markovian case, and $\alpha = \infty$ the deterministic case². We illustrate these result Figure 7, where the influence of the shape parameter on the doubling rate can be visualized. We simulate the non-Markovian division process with REGIR and fit the obtained population growth with an exponential (which result in a straight line when plotting with a logarithmic scale, Figure 7B). As expected from the analytical expression Eq.54, the obtained growth rate reduces with the shape parameter and, in the special case of $\nu = 2$, converge to $k = \ln 2$ for increasing α .

²Applying l'Hôpital's rule, It can be shown that $\lim_{x \rightarrow \infty} (xa^{1/x} - x) = \ln(a)$, see [this link](#) for details.

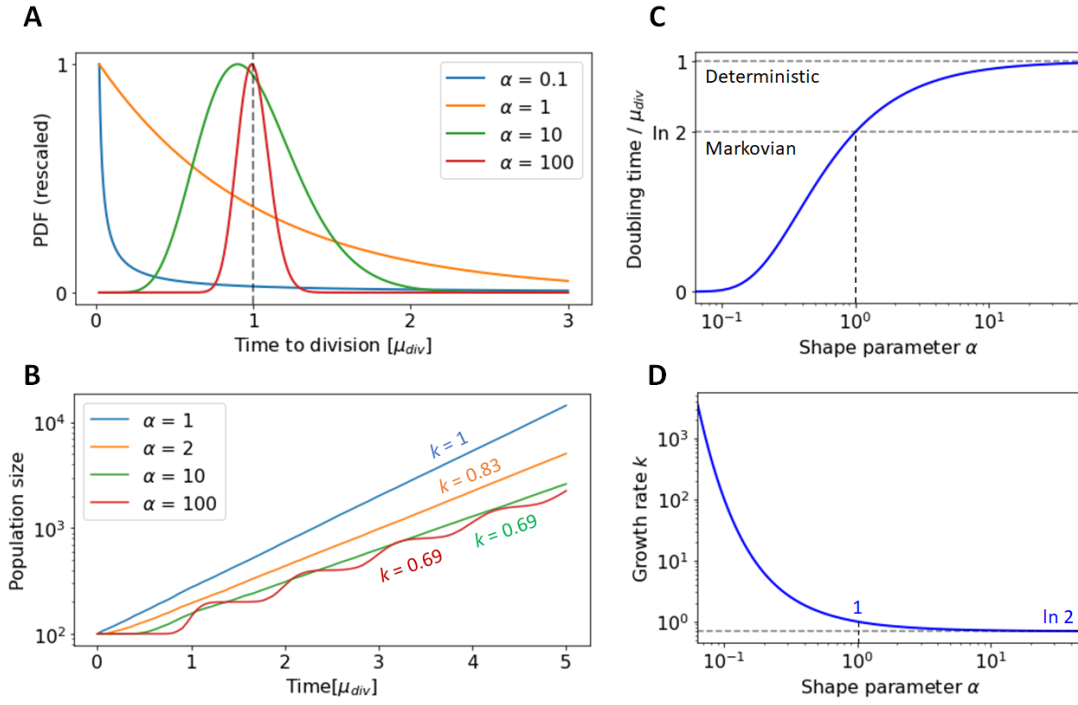


Figure 7: Population dynamics of Non-Markovian division following the equation $A \rightarrow 2A$ with a single cell interdivision time distribution following a gamma distribution of shape parameter α and mean μ_{div} . (A) PDF of gamma distributions with mean 1 and shape parameter α , rescaled for visual clarity. (B) Population growth of A for different shape parameter simulated with REGIR. The fitted exponential growth rate (k) is provided above each line. (C) Analytical ratio between the population doubling time ($t_2 = \ln(2)/k$) and the single cell average division time for different value of α . (D) Analytical growth rate of the population size for different value of α . Special cases for the Markovian ($\alpha = 1$) and deterministic ($\alpha \rightarrow \infty$) divisions are annotated.

C.2 Asymmetric division

A more complex non-Markovian system, that we describe in the main text, is asymmetric division, where a reactant A reacts to produce ν_A versions of itself as well as ν_B versions of another reactant B , following the reaction (i) $A \rightarrow \nu_A A + \nu_B B$. Then, reactant B does not divide but can differentiate into A following the reaction (ii) $B \rightarrow A$. In this setup, it was shown analytically that the population of both reactants A and B grow exponentially with the same rate k for any inter-event distribution of reactions (i) and (ii), where the growth rate k is related to the parameters ν_A and ν_B with the relation [48]

$$\mathcal{L}\{\psi_{div}\}(k) = \frac{1}{\nu_A + \nu_B \cdot \mathcal{L}\{\psi_{diff}\}(k)}, \quad [55]$$

where ψ_{div} and ψ_{diff} denote the PDF of reaction (i) and (ii), respectively. In the Markovian case, one can solve this equation with:

$$\frac{\lambda_{div}}{k + \lambda_{div}} = \frac{k + \lambda_{diff}}{\nu_A(k + \lambda_{diff}) + \nu_B \lambda_{diff}}, \quad [56]$$

which yields the quadratic equation

$$k^2 + k \cdot (\lambda_{div} - \nu_A \lambda_{div} + \lambda_{diff}) + \lambda_{div} \lambda_{diff} (1 - \nu_A - \nu_B) = 0, \quad [57]$$

where we take the positive solution for the growth rate

$$k = \frac{1}{2} \left(\lambda_{div} \nu_A - \lambda_{div} - \lambda_{diff} + \sqrt{(\lambda_{diff} + \lambda_{div} - \lambda_{div} \nu_A)^2 + 4 \lambda_{div} \lambda_{diff} (\nu_A + \nu_B - 1)} \right). \quad [58]$$

In the specific case of the reaction described in the main text ($\nu_A = \nu_B = 1$), we obtain

$$k = \frac{\lambda_{diff}}{2} \left(\sqrt{1 + 4 \frac{\lambda_{div}}{\lambda_{diff}}} - 1 \right). \quad [59]$$

In the limit $\lambda_{\text{div}} \ll \lambda_{\text{diff}}$, using the Taylor expansion $\sqrt{1+x} \sim 1+x/2$, we obtain $k = \lambda_{\text{div}}$, which recovers the symmetric case ($A \rightarrow 2A$). In this regime, differentiation ($A \rightarrow B$) is very fast compared to division, so that it can be considered to occur instantly. On the other hand, in the limit where differentiation is very slow compared to division ($\lambda_{\text{div}} \gg \lambda_{\text{diff}}$), the growth rate is given by $k = \sqrt{\lambda_{\text{div}}\lambda_{\text{diff}}}$. Finally, in the specific case of $\lambda_{\text{div}} = \lambda_{\text{diff}} = \lambda$, we obtain $k = \lambda/\varphi$ where $\varphi = \frac{1+\sqrt{5}}{2}$ is the golden ratio.

In the case of gamma or Dirac distributions, there is no simple analytical solutions for k . Thus, we use REGIR to show how the growth rate varies (Figure 8) for different combinations of distribution parameters ($\lambda_{\text{div}}, \alpha_{\text{div}}$) and ($\lambda_{\text{diff}}, \alpha_{\text{diff}}$). Interestingly, we observe that α_{div} and α_{diff} affects the growth rate in a similar manner.

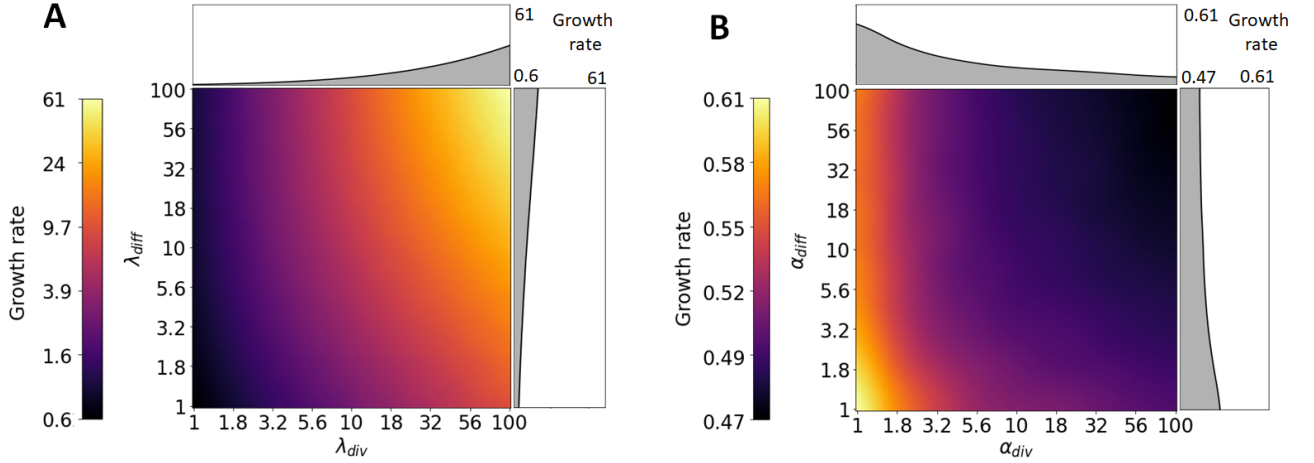


Figure 8: Growth rate of the number of cells ($N_A + N_B$) in a system of asymmetric division ($A \rightarrow A + B$ and $B \rightarrow A$), where the two processes are modeled as a gamma distribution with shape parameter ($\lambda_{\text{div}}, \alpha_{\text{div}}$) and ($\lambda_{\text{diff}}, \alpha_{\text{diff}}$). (A) Heatmap of the growth rate as a function of the processes rate ($\lambda_{\text{div}}, \lambda_{\text{diff}}$) where $\alpha_{\text{div}} = \alpha_{\text{diff}} = 1$ are kept constant. Note that growth rate axes are in logarithmic scales (B) Heatmap of the growth rate as a function of the processes shape parameters ($\alpha_{\text{div}}, \alpha_{\text{diff}}$) where $\lambda_{\text{diff}} = \lambda_{\text{div}} = 1$ are kept constant. The projection of the growth rate averaged over the differentiation and division parameter axis are plotted on the right and the top of the heatmap, respectively.

C.3 Cell inter-division time

On Figure 9 and Table 1, we show the normal, Weibull, gamma and log-normal distributions with parameters chosen to fit experimentally measured cell cycle inter event times for *Bacillus subtilis* [43] and *Escherichia coli* [44] (<https://jun.ucsd.edu/repository.php>). The log-normal distribution provides the optimal fit in all three cases as it minimizes the Earth Mover's Distance (EMD) [46].

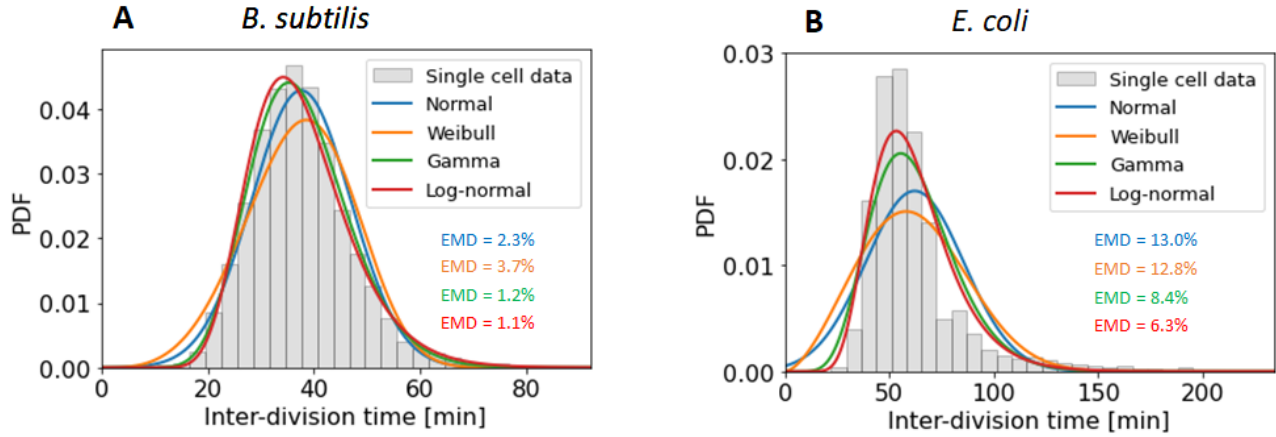


Figure 9: Measured interdivision time of (A) *Bacillus subtilis* [43] and (B) *Escherichia coli* [44] at constant temperature fitted with a normal, log-normal, gamma and Weibull distribution. The fitted distributions are quantified in term of the Earth Mover's Distance (EMD) to the measured single cell inter-division distribution.

Distribution	Exponential	Normal	Log-normal	Gamma	Weibull
EMD - <i>Bacillus subtilis</i> [43]	55.8	2.3	1.1	1.2	3.7
Optimal parameter ($1/\lambda_0$)	37.6 min	37.6 min	37.6 min	37.6 min	37.4 min
Optimal parameter (γ or α)	–	0.25	0.26	16.4	4.2
EMD - <i>Escherichia coli</i> [44]	47.4	13.0	6.3	8.4	12.8
Optimal parameter ($1/\lambda_0$)	62.0 min	62.0 min	61.7 min	62.0 min	61.8 min
Optimal parameter (γ or α)	–	0.38	0.32	9.3	2.6
EMD - <i>Caulobacter crescentus</i> [45]	64.9	2.1	1.8	1.7	5.0
Optimal parameter ($1/\lambda_0$)	72.1 min	72.1 min	72.1 min	72.1 min	71.4 min
Optimal parameter (γ or α)	–	0.12	0.12	70.8	7.1

Table 1: Fitting performance of various distributions to measured single cell inter-division time distribution of three types of bacteria dividing at constant temperature. The optimal parameters as well as the computed Earth Mover Distance (EMD) between the fitted and measured distributions are provided. EMDs are given with a confidence interval of $\pm 10\%$ of the provided value, due to stochasticity in the fitting process. Lowest EMD scores for each type of bacteria are highlighted in bold.

D Modeling stem cell differentiation

This section refers to the modeling of mouse stem cell differentiation [28] dynamics. In this experiment, cells are profiled at the single-cell level at 3 different stages of differentiation (denoted A, B, C), thus undergoing two transitions ($A \rightarrow B$ and $B \rightarrow C$). For consistency across timepoints, measured population of N_A , N_B and N_C are transformed in term of proportion $(p_A, p_B, p_C) \in [0, 1]^3$ following

$$p_A = \frac{N_A}{N_A + N_B + N_C}, \quad p_B = \frac{N_B}{N_A + N_B + N_C} \quad \text{and} \quad p_C = \frac{N_C}{N_A + N_B + N_C}. \quad [60]$$

As the population dynamics is described by proportions bounded between 0 and 1. This may bias the the optimization of the root mean square deviation (RMSD) towards ignoring variations close to very low (~ 0) and very high (~ 1) values, as a proportion of 98% will be considered closer to 99% than 50% is to 52%. To correct for this bias, we transform both simulated and measured populations with an inverse sigmoid (or logit) function (Figure 10). For experimental reasons, proportions lower than 1% or higher than 99% are considered not reliable enough (only a few hundred cells in experimental data), so we only apply the transformation within that range:

$$\begin{aligned} y_{\text{new}} &= \log\left(\frac{y}{1-y}\right) \quad \text{for } 1\% \leq y \leq 99\% \\ y_{\text{new}} &= 4.6 \quad \text{for } y > 99\% \\ y_{\text{new}} &= -4.6 \quad \text{for } y < 1\% \end{aligned} \quad [61]$$

With REGIR, we model the two differentiations processes with different choices of inter-event time distribution, and we provide in Table 2 the distribution parameters of the optimal fit to both the raw (untransformed) and logit transformed experimental data. Optimal parameters were obtained by minimizing the RMSD between the measured and simulated populations at each time point. Minimization was performed with the maxLIP0 algorithm [74], which is both parameter free and provably better than a random search. Unsurprisingly, the exponential distribution consistently yields to the highest RMSD, while the normal, log-normal and gamma output similarly low RMSD. On the other hand, the Weibull distribution consistently output higher RMSD than other distributions for both the untransformed and transformed data.

Distribution	Exponential	Normal	Log-normal	Gamma	Weibull
RMSD (sigmoid transformed data)	2.1	0.38	0.39	0.35	0.69
Optimal parameter ($1/\lambda_1$)	29.4 h	31.9 h	32.3 h	31.9 h	32.2 h
Optimal parameter ($1/\lambda_2$)	66.7 h	66.7 h	62.9 h	65.4 h	63.3 h
Optimal parameter (γ_1 or α_1)	–	0.24	0.21	20.2	4.3
Optimal parameter (γ_2 or α_2)	–	0.15	0.15	38.7	4.8
RMSD (untransformed data)	0.22	0.017	0.014	0.019	0.039
Optimal parameter ($1/\lambda_1$)	31.9 h	32.1 h	31.6 h	29.5 h	31.8 h
Optimal parameter ($1/\lambda_2$)	63.7 h	59.2 h	59.9 h	61.0 h	58.8 h
Optimal parameter (γ_1 or α_1)	–	0.27	0.27	27.6	4.65
Optimal parameter (γ_2 or α_2)	–	0.050	0.083	39.3	4.94

Table 2: Root mean square deviation (RMSD) between simulated and measured stem cell differentiation data for both the raw and sigmoid transformed data. Lowest RMSD scores are highlighted in bold.

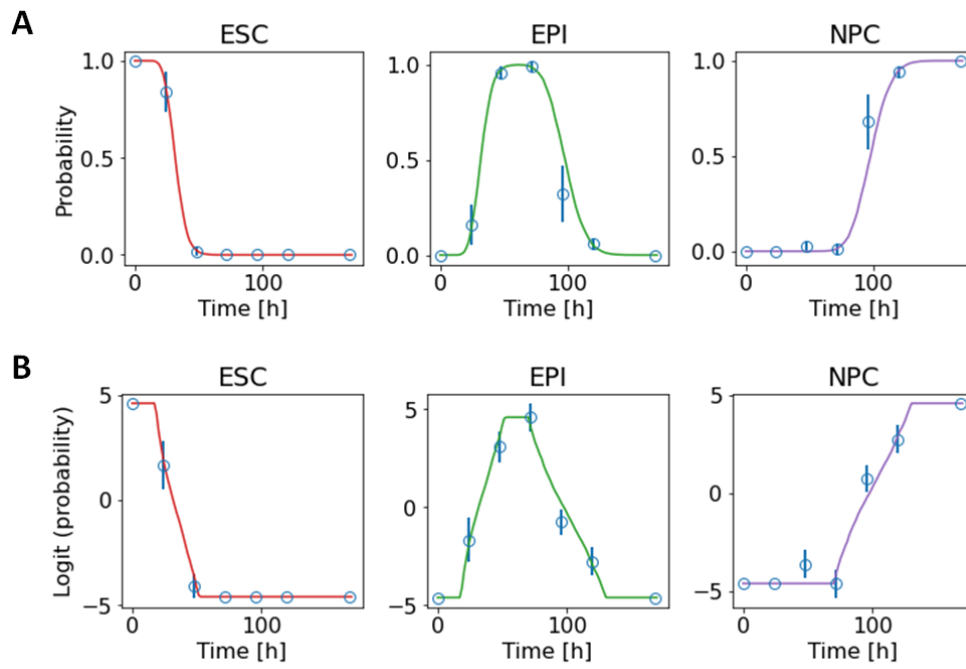


Figure 10: Normalized stem cell population as a function of time for the three stages of differentiations following the reactions $ESC \rightarrow EPI$ and $EPI \rightarrow NPC$. The blue points represent the mean and standard deviation of the stem cell populations measured at different time points [28], and the solid lines depict the population dynamics averaged over 1000 REGIR simulation, with differentiation modelled as the best fitting gamma distribution. Results are shown for (A) the untransformed and (B) transformed probabilities with an inverse sigmoid (or logit) function.

E Non-Markovian dynamics of RNA transcription

This section provide additional information regarding the two steps model of RNA transcription described in the main text. As a reminder, we consider a promoter switching between an ON and an OFF state with gamma inter-event distributions parametrized by $(\lambda_{\text{on}}, \alpha_{\text{on}})$ and $(\lambda_{\text{off}}, \alpha_{\text{off}})$. Some mRNA may be produced only if the promoter state is ON, with a gamma inter-event distribution $(\lambda_{\text{prod}}, \alpha_{\text{prod}})$. The mRNA then degrades at a constant rate λ_{deg} . The system is initialized with a promoter in an OFF state and a count of 0 mRNA.

E.1 Oscillations of mRNA dynamics

Modeling RNA transcription with non-Markovian processes may results into predictable oscillations of averaged mRNA counts before the steady state is reached, a phenomenon that is not observed in the Markovian case. For example, in the specific case of a deterministic promoter transition (promoter activation and deactivation modeled as Dirac distributions), the promoter oscillates between the G_{on} and G_{off} state indefinitely with a period of $T = 1/\lambda_{\text{on}} + 1/\lambda_{\text{off}}$, which results in oscillations in mRNA count with the same period. Adding some stochasticity to the promoter transition results in a decay of the G_{on} and G_{off} probability oscillation amplitude, until it converges to the steady state value and no more amplitudes can be observed (Figure 11A&B). Interestingly, the more *stochasticity* is added to the promoter transition reaction (decreasing shape parameter α_{on} and α_{off}), the faster the oscillation decays (Figure 11B&C). In the case of Markovian mRNA transcription ($\alpha_{\text{on}} = \alpha_{\text{off}} = 1$), the system reaches directly its steady state after a single period T and oscillations are not observed (Figure 11A).

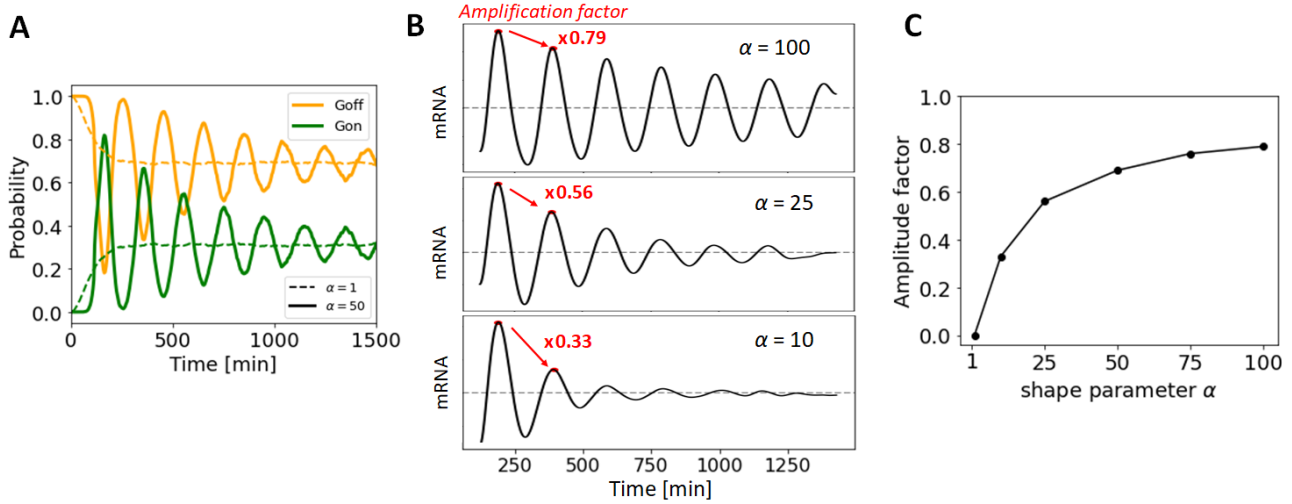


Figure 11: Oscillations in non-Markovian mRNA transcription dynamics where we set $\alpha = \alpha_{\text{on}} = \alpha_{\text{off}}$ for simplicity. (A) Time dependent probability that the promoter is in the on or off states for both the Markovian ($\alpha = 1$, dashed line) and non Markovian case ($\alpha = 50$, solid line) at each time point, obtained after averaging over 10k simulations. (B) Time evolution of mRNA count averaged over 10k REGIR simulations for different shape parameters α . For visual clarity, only the time interval where the mRNA count oscillate around its steady state value (dashed line) is plotted. The observed factor at which the oscillation amplitude decays between each period is shown in red. (C) Dependency of the shape parameter α on the oscillation amplification factor (amplitude of the second peak divided by the amplitude of the first peak) of averaged mRNA counts.

E.2 Modeling the reaction to stimuli in RNA transcription

Non steady state RNA transcription dynamics are not straight forward to observe directly experimentally. A possibility is to study the behavior of RNA dynamics after stimuli by the epidermal growth factor (EGF) or lipopolysaccharide (LPS), which initiate well characterized signaling cascades that culminate in orchestrated transcriptional responses [58]. After the stimuli, the system take some times to reach its new steady state, which results in observable non-steady state dynamics shortly after the stimuli. It was shown that the stimuli may affect all rates involved in RNA transcription ($\lambda_{\text{on}}, \lambda_{\text{off}}, \lambda_{\text{deg}}$) [58] (Figure 12B). To avoid introducing too many new parameters in our model to incorporate the stimuli, we keep λ_{deg} and λ_{off} constant, and we set the promoter activation rate $\lambda_{\text{on}}(t)$ to change with time as a function of two terms:

$$\lambda_{\text{on}}(t) = \lambda_{\text{on}}^{\text{decay}}(t) + \lambda_{\text{on}}^{\text{peak}}(t). \quad [62]$$

The first one is a progressive decay (modeled with a sigmoid function) from its value before the stimuli (λ_A) to its new value (λ_B) as

$$\lambda_{\text{on}}^{\text{decay}}(t) = (\lambda_A - \lambda_B) \cdot \frac{e^{-b(t-t_0)}}{1 + e^{-b(t-t_0)}} + \lambda_B \quad [63]$$

where t refers to the time elapsed since the stimuli. Additionally, we also add a second term to simulate the short term peak induced by the stimuli, as introduced in original study [58]:

$$\lambda_{\text{on}}^{\text{peak}}(t) = a_1 \frac{(t/t_p)^{n_1}}{(1 + t/t_p)^{n_2}} \cdot \text{with } n_1 < n_2 \quad [64]$$

This peak induce a very short spike in the λ_{on} rate (Figure 12B) and cause the system to leave its steady state to enter non-Markovian dynamics. To make the parameter optimization easier, we fix the parameters $t_p = 5$ min, $n_1 = 2$ and $n_2 = 4$ for all our simulation. On the other hand, we leave the parameter a_1 as variable since it reflects the amplitude of the peak and thus the oscillation amplitudes of RNA transcription.

The modeling of stimuli is performed by first simulating the system before the stimuli until its steady state is reached ($\lambda_{\text{on}} = \lambda_A$), and then re-initializing $t = 0$ and the promoter to its off state (Figure 12A). We adjust the models parameters to optimize the fit to experimental data for the genes CREG1, DDB2, SLC7A5, and NFYC (Figure 12C). For all simulation, we constrain $\alpha_{\text{on}} = \alpha_{\text{off}} = \alpha$ and $\alpha_{\text{prod}} = 1$ to facilitate the parameter fit. Note that with these constraints, the non-Markovian model only have one more parameter of freedom (α) than the Markovian model. For each gene, parameters (α , λ_A , λ_B , b , t_0 and a_1) are fitted with the maxLIPO algorithm [74] by minimizing the RMSD between the REGIR output of 1000 simulations and the experimental data (Table 3). Note that since the dataset involve fold-change of mRNA since $t = 0$ rather than absolute mRNA count, it is not possible to fit parameters such as λ_{off} or λ_{prod} , so we set them to constant values for all simulations ($\lambda_{\text{off}} = 4\lambda_{\text{deg}}$ and $\lambda_{\text{prod}} = 25\lambda_{\text{deg}}$). Also, while $\lambda_{\text{on}}(t = 0) = \lambda_A$ can be inferred from the oscillation period in the non-Markovian model (REGIR), it is not possible to obtain it in the Markovian case (SG) as there is no oscillations (marked as X in Table 3).

Interestingly, several of the studied genes revealed oscillations in their mRNA expression after the stimuli that could not be replicated accurately by the Markovian model (e.g. RMSD = 0.016 for SLC7A5). On the other hand, REGIR was able to reproduce the oscillations accurately (e.g. RMSD = 0.0083 for SLC7A5). Strikingly, the genes where the most significant difference was observed between the non-Markovian and Markovian model were the

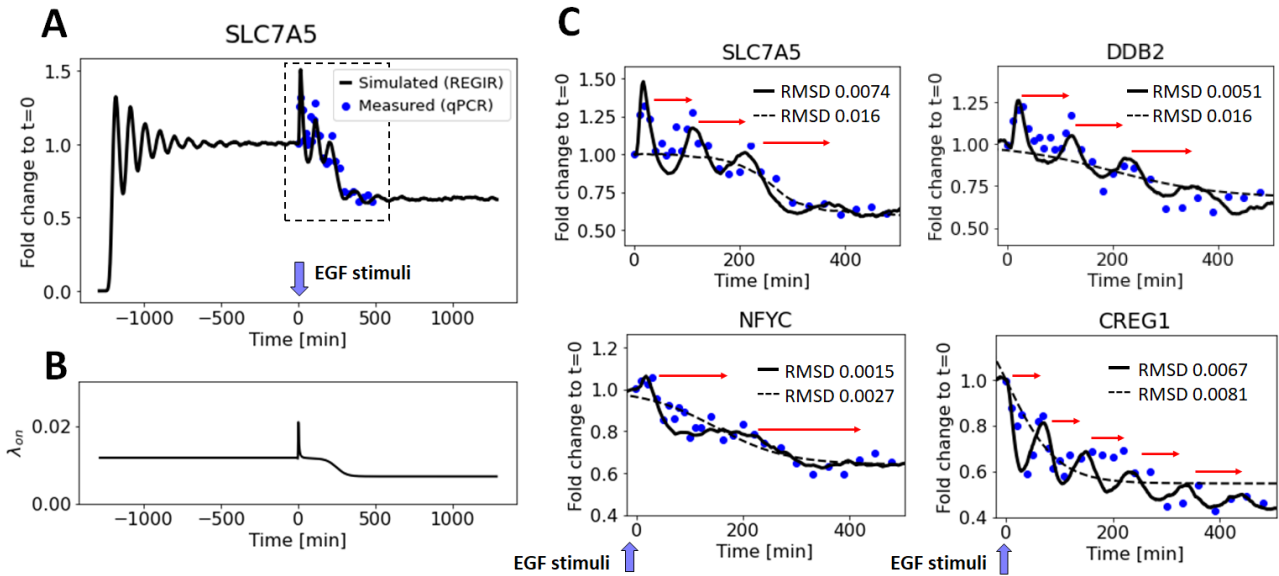


Figure 12: (A) Simulated mRNA gene expression of SLC7A5 normalized by its average expression at the time of stimulation, averaged over 10k simulation. We can clearly distinguish two phases, where the mRNA dynamics reaches first reaches its steady state and then reacts to the stimuli. (B) Time evolution of the simulated promoter activation rate of SLC7A5 (λ_{on}) before ($t < 0$) and after ($t > 0$) the EGF stimuli. (C) mRNA gene expression of different genes normalized by their average expression at the time of stimulation, where the measured expression [58] by quantitative PCR (qPCR) are compared to simulated RNA expression averaged over 10k simulations with optimal parameter fit. The simulation is provided for both REGIR (solid line) and the Markovian model (SG, dashed line). Red arrow highlight the increase in oscillation period caused by the decrease of λ_{on} .

one with the highest oscillation amplitudes. Another interesting aspect is the gradual increasing period of the oscillations, which indicate a progressive reduction in the promoter activation rate (red arrows on Figure 12C).

	RMSD	λ_A	λ_B	b [1/min]	t_0 [min]	a_1	α
CREG1 (SG)	0.0081	X	$0.45 \cdot \lambda_A$	0.004	0	X	
CREG1 (REGIR)	0.0067	$\lambda_{\text{off}}/4.5$	$0.45 \cdot \lambda_A$	0.006	0	-1.2	40
DDB2 (SG)	0.016	X	$0.66 \cdot \lambda_A$	0.029	214	X	
DDB2 (REGIR)	0.0051	$\lambda_{\text{off}}/9$	$0.66 \cdot \lambda_A$	0.012	250	1	60
NFYC (SG)	0.0027	X	$0.64 \cdot \lambda_A$	0.015	150	X	
NFYC (REGIR)	0.0015	$\lambda_{\text{off}}/18$	$0.64 \cdot \lambda_A$	0.008	160	0.55	15
SLC7A (SG)	0.016	X	$0.63 \cdot \lambda_A$	0.041	270	X	
SLC7A (REGIR)	0.0074	$\lambda_{\text{off}}/9.6$	$0.63 \cdot \lambda_A$	0.035	270	1.3	26

Table 3: Optimal parameters and root mean square deviation (RMSD) between the simulated and measured mRNA time resolved gene expression fold changes after EGF stimulation [58]. Results are provided for both the SG and REGIR model, each averaged over 1000 simulations. Best RMSD scores for each genes are highlighted in bold. Parameters marked with | indicate that it is not applicable in the model. Parameters marked with X mean that the model is insensitive to its value, so it's irrelevant in the context of optimization.

E.3 Phase diagrams and sensitivity analysis of the steady state mRNA count distribution

In the main text, we performed a variance-based sensitivity analysis of the coefficient of variation ($CV = \text{std}/\text{mean}$) of the steady state mRNA distribution. In Figure 13, we provide the same sensitivity analysis for the mean, and the differential entropy H . Intuitively, H measures the randomness of a random variable and the number of bits required to describe it. Formally, H is computed as a generalization of the Shannon entropy to continuous distributions:

$$H(X) = - \int_{\mathcal{X}} f(x) \log f(x) dx. \quad [65]$$

Numerically, we compute it by discretizing the mRNA distribution into N_b bins and computing the histogram. As the choice of the number of bin can affect the measure, we chose the same number of bins $N_b = 25$ for all entropy estimations.

The sensitivity analysis of the mean steady state mRNA distribution is consistent with previous analytical results showing that, in the steady state, the mean mRNA distribution only depends on the mean inter-event time distribution [35], and thus, is not influenced by the shape parameters. We also compute phase diagrams of the mean, CV and entropy of mRNA distribution, where the impact of variation in the parameters can be assessed visually. On Figure 14, we show it for the combinations $(\alpha_{\text{on}} = 1, \alpha_{\text{off}} = 1)$, $(\alpha_{\text{on}} = 10, \alpha_{\text{off}} = 1)$, $(\alpha_{\text{on}} = 1, \alpha_{\text{off}} = 10)$ and $(\alpha_{\text{on}} = 10, \alpha_{\text{off}} = 10)$. We observe that, although sensitive, changing the shape parameters $(\alpha_{\text{on}}, \alpha_{\text{on}})$ do not affect significantly the phase diagrams of the CV, but rather lower all CV values by a constant factor (0.4 in this case). As for the entropy, the variations across the depicted parameter space is relatively small except for a low λ_{on} where it shows a drastic decrease. We note that the contour plot in the phase diagrams are relatively noisy due to the low variation of the entropy in the simulated parameter range.

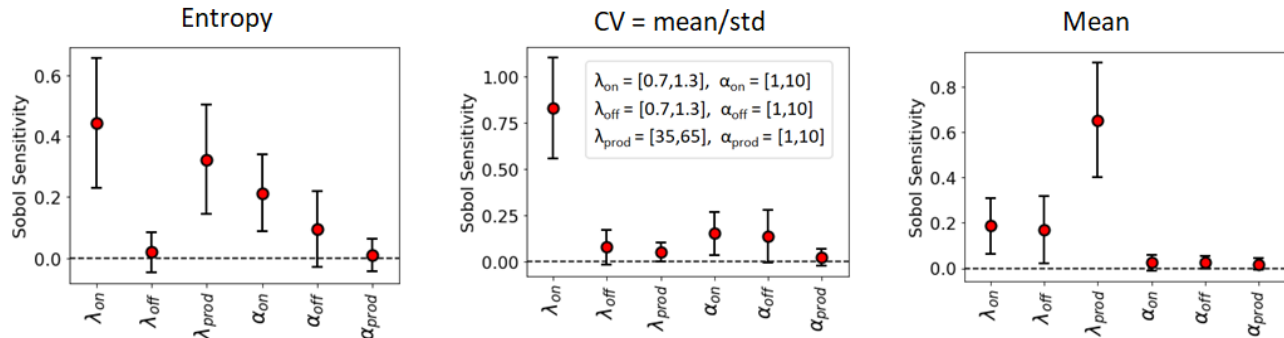


Figure 13: Sobol variance-based sensitivity analysis of the Mean, CV and entropy of the steady state single cell mRNA distribution generated by the two step model, with a grid of 128 points per parameters. The parameter bounds used for all analysis are given in the middle box.

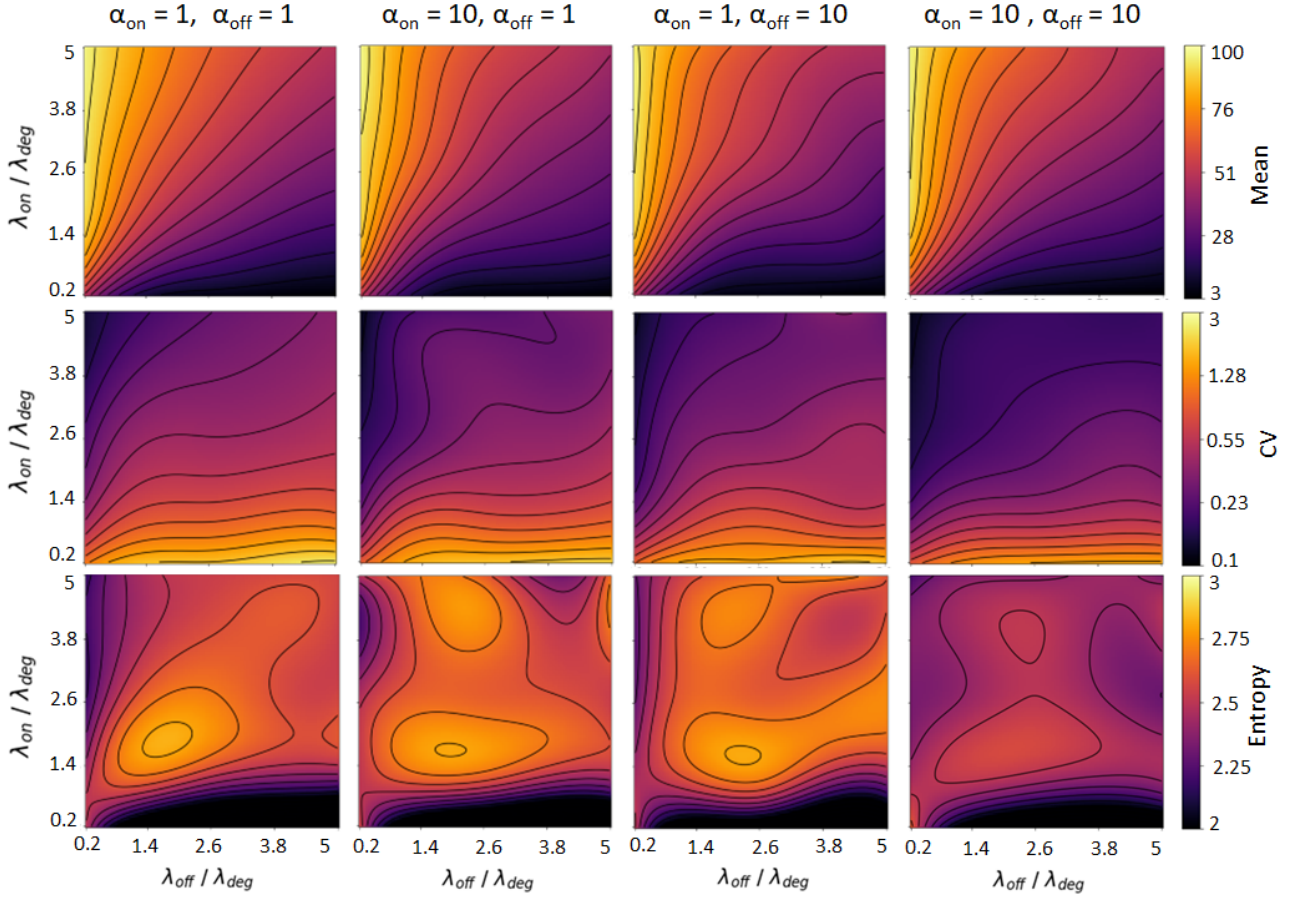


Figure 14: Mean, CV and entropy phase diagram of the steady state single cell mRNA distribution for different combination of shape parameter, i.e. the Markovian ($\alpha_{\text{on}} = \alpha_{\text{off}} = 1$) and non-Markovian cases ($\alpha_{\text{on}} \neq 1, \alpha_{\text{off}} \neq 1$). The heat map were generated with a 2D cubic interpolation of a 10x10 parameter grid, with REGIR results averaged over 1000 simulations. Parameters $\alpha_{\text{prod}} = 1$ and $\lambda_{\text{prod}} = 100$ were fixed for all simulations.

F EMD & REGIR accuracy

F.1 Baseline EMD distance

The earth mover's distance (EMD) [46] is a measure of the distance between two probability distributions, which reflects the minimal amount of *work* that must be used to transform one distribution into the other. In practice, because the two distributions are often discrete points sampled from a *theoretical* distribution, the EMD will always have an intrinsic non-zero value even if $P = Q$. This come from the fact that sampled points from equivalent distributions will not be strictly equal. This background varies dramatically depending on the number of point sampled, and tends to zero as the number of sampled points increases. As an example, we show Figure 15A the intrinsic EMD distance between two equal gamma distributions of shape parameter $\alpha = 6$. In the main article, we work with an EMD distance defined with 10k samplings. Thus, we define the baseline EMD of 1%, as it corresponds to the mean plus one standard deviation for that number of sampling points.

Importantly, the baseline EMD is also affected by the variance of the distribution and thus shape parameter (Figure 15B). On one extreme, the Dirac distribution would always yield an EMD of 0 since all sampled point would be the same. On the other side, very long tailed distribution like Cauchy which results in a few outliers point that will vastly increase the EMD.

F.2 Trade-off between accuracy and computational cost in REGIR

As in all simulation frameworks, there is a trade-off between accuracy and running time. To control for this trade-off, REGIR introduces a new parameter f that enables a user to select a fixed accuracy, while maintaining the complexity at similar levels to Markovian algorithms. Given user-defined constraints about the desired accuracy or maximum running time, f should be kept as low as possible to optimize the trade-off between accuracy and

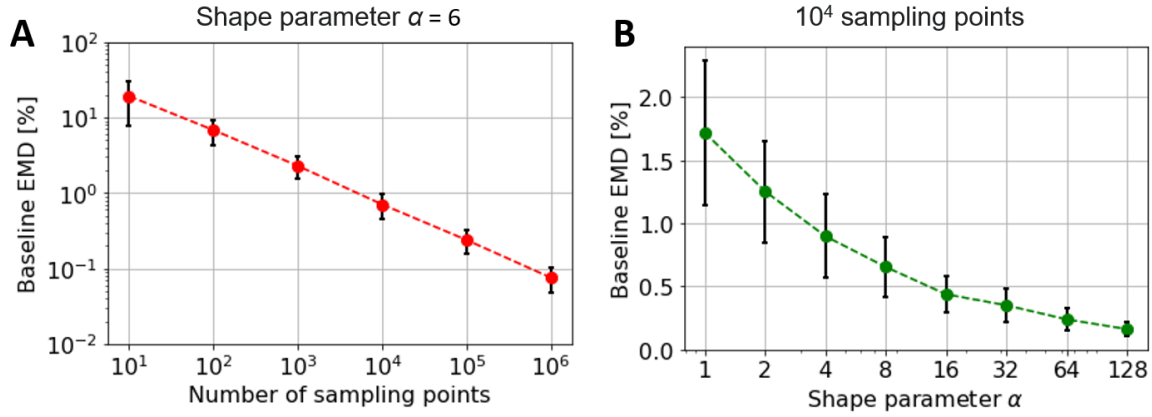


Figure 15: Baseline EMD distance for the gamma distribution. It is depicted as a function of (A) the sampling size, with a distribution of shape parameters $\alpha = 6$ and (B) the shape parameter of the gamma distribution, with 10k sampling points. The baseline EMD values are averaged over 100 occurrences and the error bars represent the standard deviation.

computational cost. We remind that the time to next event in REGIR is computed as $\Delta t = \frac{\ln(1/u)}{N \cdot \lambda_{\max}}$ and such that the inequality $\Delta t \leq \frac{\ln(1/u)}{f \cdot \lambda_0}$ is always verified. While the simulation accuracy is improved when Δt is reduced, the computational time, which scales linearly with Δt , increases.

On Figure 16A, we visualize how the computational cost scales with the number of reactant and the accuracy parameter f . As expected, the time per simulation increases as the number of reactants (N) or the accuracy parameter (f) increases. Still, increasing f does not affect the computational time when $f < N$. That's because in this case, the inequality

$$\max_{\{j \in [1, N]\}} \lambda_j(t_j) \geq f \cdot \frac{\lambda_0}{N} \quad [66]$$

is always verified with high probability, so that

$$\lambda_{\max} = \max_{\{j \in [1, N]\}} \lambda_j(t_j) \quad [67]$$

regardless of the value of f (provided that $f < N$)

Regarding the simulation accuracy (Figure 16A), we observe that the EMD to the theoretical distribution decreases as f or N increases. Here we observe that $f \geq 32$ is enough to reach the baseline EMD regardless of the number of reactants. Importantly, for a few reactants (≥ 2), the user can define $f = 4$ and still gets an accuracy below the baseline, so the optimal f depends on the number of reactants in the model. Finally, here we defined our baseline EMD as computed from two equal distributions with 10k sampling. For 100k samplings, the baseline EMD becomes 0.2% which would then requires around $f \sim 200$ (extrapolated from the trend of Figure 16B for EMD > baseline), thus increasing the computational cost roughly by an order of magnitude.

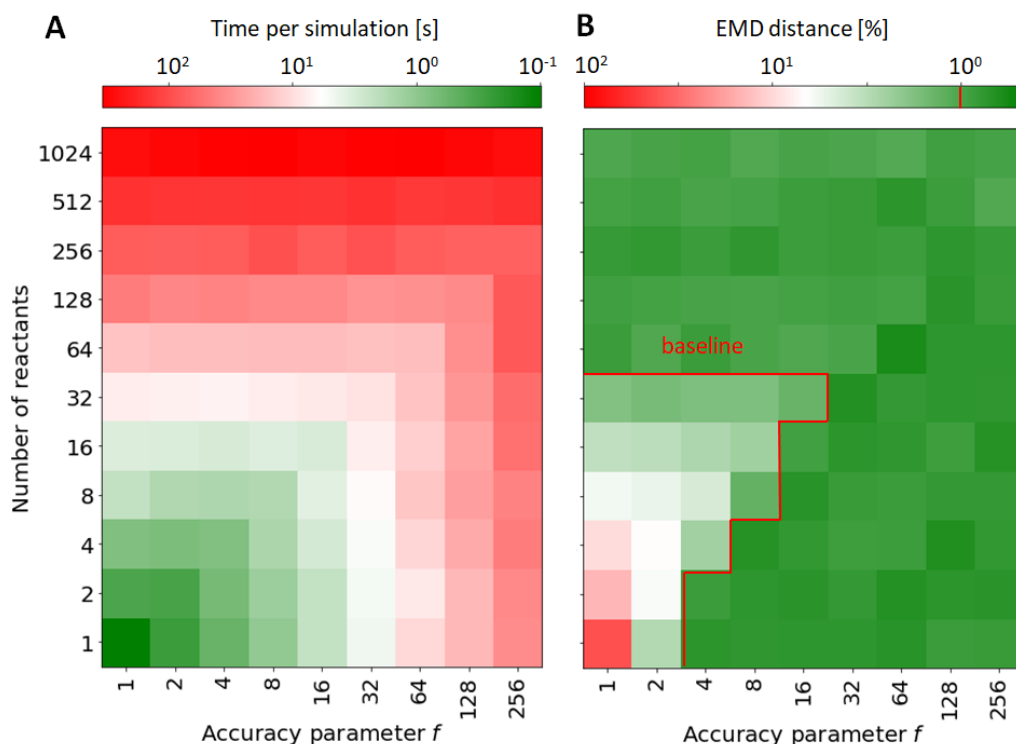


Figure 16: Trade-off between computational cost and accuracy. The toy reaction $A \rightarrow \emptyset$ is simulated with a gamma inter-event time distribution with parameters ($\lambda_0 = 1$, $\alpha = 6$). We display the heatmap of (A) the computational time for one simulation and (B) the EMD distance from the theoretical distribution. All values are averaged over 100 simulations, and EMD distances are given with a $\pm 10\%$ confidence interval. The red lines mark the border where the EMD becomes below the baseline EMD (defined as 1%).

References

- [1] Sheldon M Ross et al. *Stochastic processes*. Vol. 2. Wiley New York, 1996.
- [2] Nicolaas Godfried Van Kampen. *Stochastic processes in physics and chemistry*. Vol. 1. Elsevier, 1992.
- [3] Yang Cao and David C Samuels. “Discrete stochastic simulation methods for chemically reacting systems”. In: *Methods in enzymology* 454 (2009), pp. 115–140.
- [4] Ping Yan. “Distribution theory, stochastic processes and infectious disease modelling”. In: *Mathematical epidemiology*. Springer, 2008, pp. 229–293.
- [5] Masaaki Kijima. *Stochastic processes with applications to finance*. Chapman and Hall/CRC, 2002.
- [6] Yi-Ting Tseng et al. “Forecasting the seasonal pollen index by using a hidden Markov model combining meteorological and biological factors”. In: *Science of the Total Environment* 698 (2020), p. 134246.
- [7] Maria Rodriguez Martinez et al. “Messenger RNA fluctuations and regulatory RNAs shape the dynamics of a negative feedback loop”. In: *Physical Review E* 81.3 (2010), p. 031924.
- [8] Takeyuki Hida. “Brownian motion”. In: *Brownian motion*. Springer, 1980, pp. 44–113.
- [9] Daniel T Gillespie. “A general method for numerically simulating the stochastic time evolution of coupled chemical reactions”. In: *Journal of computational physics* 22.4 (1976), pp. 403–434.
- [10] Daniel T Gillespie. “Exact stochastic simulation of coupled chemical reactions”. In: *The journal of physical chemistry* 81.25 (1977), pp. 2340–2361.
- [11] Graziela P Figueredo et al. “Comparing stochastic differential equations and agent-based modelling and simulation for early-stage cancer”. In: *PloS one* 9.4 (2014), e95150.
- [12] Adam Arkin, John Ross, and Harley H McAdams. “Stochastic kinetic analysis of developmental pathway bifurcation in phage λ -infected *Escherichia coli* cells”. In: *Genetics* 149.4 (1998), pp. 1633–1648.
- [13] Marcel Jan Thomas et al. “A probabilistic model of the germinal center reaction”. In: *Frontiers in immunology* 10 (2019), p. 689.

- [14] Aurélien Péliissier et al. “Computational model reveals a stochastic mechanism behind germinal center clonal bursts”. In: *Cells* 9.6 (2020), p. 1448.
- [15] Christian L Vestergaard and Mathieu Géniois. “Temporal gillespie algorithm: Fast simulation of contagion processes on time-varying networks”. In: *PLoS computational biology* 11.10 (2015).
- [16] Lei Sun et al. “Stochastic gene expression influences the selection of antibiotic resistance mutations”. In: *Molecular biology and evolution* 37.1 (2020), pp. 58–70.
- [17] Lawrence Rabiner and Biinghwang Juang. “An introduction to hidden Markov models”. In: *ieee assp magazine* 3.1 (1986), pp. 4–16.
- [18] Byung-Jun Yoon. “Hidden Markov models and their applications in biological sequence analysis”. In: *Current genomics* 10.6 (2009), pp. 402–415.
- [19] RC Rose and BH Juang. “Hidden Markov models for speech and signal recognition.” In: *Electroencephalography and Clinical Neurophysiology. Supplement* 45 (1996), pp. 137–152.
- [20] Nguyet Nguyen and Dung Nguyen. “Hidden markov model for stock selection”. In: *Risks* 3.4 (2015), pp. 455–473.
- [21] C Bracken, B Rajagopalan, and E Zagona. “A hidden Markov model combined with climate indices for multidecadal streamflow simulation”. In: *Water Resources Research* 50.10 (2014), pp. 7836–7846.
- [22] Gregory AL White et al. “Demonstration of non-Markovian process characterisation and control on a quantum processor”. In: *Nature Communications* 11.1 (2020), pp. 1–10.
- [23] Thomas Guérin, Olivier Bénichou, and Raphaël Voituriez. “Non-Markovian polymer reaction kinetics”. In: *Nature chemistry* 4.7 (2012), pp. 568–573.
- [24] Cihan Ayaz et al. “Non-Markovian modeling of protein folding”. In: *Proceedings of the National Academy of Sciences* 118.31 (2021), e2023856118.
- [25] Hadrien Vroylandt et al. “Likelihood-based non-Markovian models from molecular dynamics”. In: *Proceedings of the National Academy of Sciences* 119.13 (2022), e2117586119.
- [26] Benjamin Lickert and Gerhard Stock. “Modeling non-Markovian data using Markov state and Langevin models”. In: *The Journal of Chemical Physics* 153.24 (2020), p. 244112.
- [27] Dmitri Bratsun et al. “Delay-induced stochastic oscillations in gene regulation”. In: *Proceedings of the National Academy of Sciences* 102.41 (2005), pp. 14593–14598.
- [28] Patrick S Stumpf et al. “Stem cell differentiation as a non-Markov stochastic process”. In: *Cell Systems* 5.3 (2017), pp. 268–282.
- [29] Zhixing Cao and Ramon Grima. “Analytical distributions for detailed models of stochastic gene expression in eukaryotic cells”. In: *Proceedings of the National Academy of Sciences* 117.9 (2020), pp. 4682–4692.
- [30] Roland Baddeley et al. “Responses of neurons in primary and inferior temporal visual cortices to natural scenes”. In: *Proceedings of the Royal Society of London. Series B: Biological Sciences* 264.1389 (1997), pp. 1775–1783.
- [31] Zhi-Qiang Jiang et al. “Calling patterns in human communication dynamics”. In: *Proceedings of the National Academy of Sciences* 110.5 (2013), pp. 1600–1605.
- [32] Kun Zhao and Ginestra Bianconi. “Social interactions model and adaptability of human behavior”. In: *Frontiers in physiology* 2 (2011), p. 101.
- [33] Albert-Laszlo Barabasi. “The origin of bursts and heavy tails in human dynamics”. In: *Nature* 435.7039 (2005), pp. 207–211.
- [34] Alvaro Corral. “Long-term clustering, scaling, and universality in the temporal occurrence of earthquakes”. In: *Physical Review Letters* 92.10 (2004), p. 108501.
- [35] Zihao Wang, Zhenquan Zhang, and Tianshou Zhou. “Analytical results for non-markovian models of bursty gene expression”. In: *Physical Review E* 101.5 (2020), p. 052406.
- [36] Marian Boguná et al. “Simulating non-Markovian stochastic processes”. In: *Physical Review E* 90.4 (2014), p. 042108.
- [37] Naoki Masuda and Luis EC Rocha. “A Gillespie algorithm for non-Markovian stochastic processes”. In: *SIAM Review* 60.1 (2018), pp. 95–115.
- [38] Gerrit Großmann, Luca Bortolussi, and Verena Wolf. “Efficient simulation of non-Markovian dynamics on complex networks”. In: *Plos one* 15.10 (2020), e0241394.

- [39] Vo Hong Thanh, Corrado Priami, and Roberto Zunino. “Efficient rejection-based simulation of biochemical reactions with stochastic noise and delays”. In: *The Journal of chemical physics* 141.13 (2014), 10B602_1.
- [40] Guillaume St-Onge et al. “Efficient sampling of spreading processes on complex networks using a composition and rejection algorithm”. In: *Computer physics communications* 240 (2019), pp. 30–37.
- [41] Renyan Jiang and DNP Murthy. “A study of Weibull shape parameter: Properties and significance”. In: *Reliability Engineering & System Safety* 96.12 (2011), pp. 1619–1626.
- [42] Jue D Wang and Petra A Levin. “Metabolism, cell growth and the bacterial cell cycle”. In: *Nature Reviews Microbiology* 7.11 (2009), pp. 822–827.
- [43] John T Sauls et al. “Control of *Bacillus subtilis* replication initiation during physiological transitions and perturbations”. In: *MBio* 10.6 (2019), e02205–19.
- [44] Fangwei Si et al. “Mechanistic origin of cell-size control and homeostasis in bacteria”. In: *Current Biology* 29.11 (2019), pp. 1760–1770.
- [45] Srividya Iyer-Biswas et al. “Scaling laws governing stochastic growth and division of single bacterial cells”. In: *Proceedings of the National Academy of Sciences* 111.45 (2014), pp. 15912–15917.
- [46] Yossi Rubner, Carlo Tomasi, and Leonidas J Guibas. “A metric for distributions with applications to image databases”. In: *Sixth International Conference on Computer Vision (IEEE Cat. No. 98CH36271)*. IEEE, 1998, pp. 59–66.
- [47] Jennifer C England et al. “Global regulation of gene expression and cell differentiation in *Caulobacter crescentus* in response to nutrient availability”. In: *Journal of bacteriology* 192.3 (2010), pp. 819–833.
- [48] Farshid Jafarpour et al. “Bridging the timescales of single-cell and population dynamics”. In: *Physical Review X* 8.2 (2018), p. 021007.
- [49] Alejandro Sánchez Alvarado and Shinya Yamanaka. “Rethinking differentiation: stem cells, regeneration, and plasticity”. In: *Cell* 157.1 (2014), pp. 110–119.
- [50] Ian Chambers et al. “Nanog safeguards pluripotency and mediates germline development”. In: *Nature* 450.7173 (2007), pp. 1230–1234.
- [51] Michael B Elowitz et al. “Stochastic gene expression in a single cell”. In: *Science* 297.5584 (2002), pp. 1183–1186.
- [52] Vahid Shahrezaei and Peter S Swain. “Analytical distributions for stochastic gene expression”. In: *Proceedings of the National Academy of Sciences* 105.45 (2008), pp. 17256–17261.
- [53] David M Suter et al. “Mammalian genes are transcribed with widely different bursting kinetics”. In: *science* 332.6028 (2011), pp. 472–474.
- [54] Srividya Iyer-Biswas, Fernand Hayot, and Ciriya Jayaprakash. “Stochasticity of gene products from transcriptional pulsing”. In: *Physical Review E* 79.3 (2009), p. 031911.
- [55] Anton JM Larsson et al. “Genomic encoding of transcriptional burst kinetics”. In: *Nature* 565.7738 (2019), pp. 251–254.
- [56] Jong Kyoung Kim and John C Marioni. “Inferring the kinetics of stochastic gene expression from single-cell RNA-sequencing data”. In: *Genome biology* 14.1 (2013), pp. 1–12.
- [57] Yulei Wang et al. “Precision and functional specificity in mRNA decay”. In: *Proceedings of the National Academy of Sciences* 99.9 (2002), pp. 5860–5865.
- [58] Amit Zeisel et al. “Coupled pre-mRNA and mRNA dynamics unveil operational strategies underlying transcriptional responses to stimuli”. In: *Molecular systems biology* 7.1 (2011), p. 529.
- [59] Nacho Molina et al. “Stimulus-induced modulation of transcriptional bursting in a single mammalian gene”. In: *Proceedings of the National Academy of Sciences* 110.51 (2013), pp. 20563–20568.
- [60] Ilya M Sobol. “Global sensitivity indices for nonlinear mathematical models and their Monte Carlo estimates”. In: *Mathematics and computers in simulation* 55.1-3 (2001), pp. 271–280.
- [61] Kevin R Sanft and Hans G Othmer. “Constant-complexity stochastic simulation algorithm with optimal binning”. In: *The Journal of chemical physics* 143.7 (2015), 08B609_1.
- [62] Michael Hucka et al. “The systems biology markup language (SBML): a medium for representation and exchange of biochemical network models”. In: *Bioinformatics* 19.4 (2003), pp. 524–531.
- [63] Rahuman S Malik-Sheriff et al. “BioModels—15 years of sharing computational models in life science”. In: *Nucleic acids research* 48.D1 (2020), pp. D407–D415.

- [64] Tomás Aquino and Marco Dentz. “Chemical Continuous Time Random Walks”. en. In: *Physical Review Letters* 119.23 (Dec. 2017), p. 230601. issn: 0031-9007, 1079-7114.
- [65] Jiajun Zhang and Tianshou Zhou. “Markovian approaches to modeling intracellular reaction processes with molecular memory”. In: *Proceedings of the National Academy of Sciences* 116.47 (2019), pp. 23542–23550.
- [66] Qingchao Jiang et al. “Neural network aided approximation and parameter inference of non-Markovian models of gene expression”. In: *Nature communications* 12.1 (2021), pp. 1–12.
- [67] Ulysse Herbach et al. “Inferring gene regulatory networks from single-cell data: a mechanistic approach”. In: *BMC systems biology* 11.1 (2017), pp. 1–15.
- [68] Onno Boxma et al. “On/off storage systems with state-dependent input, output, and switching rates”. In: *Probability in the Engineering and Informational Sciences* 19.1 (2005), pp. 1–14.
- [69] Khashayar Pakdaman, Michele Thieullen, and Gilles Wainrib. “Fluid limit theorems for stochastic hybrid systems with application to neuron models”. In: *Advances in Applied Probability* 42.3 (2010), pp. 761–794.
- [70] Tatiana Filatova, J Gary Polhill, and Stijn Van Ewijk. “Regime shifts in coupled socio-environmental systems: Review of modelling challenges and approaches”. In: *Environmental modelling & software* 75 (2016), pp. 333–347.
- [71] Yuxin Deng and Wenjie Du. “The Kantorovich metric in computer science: A brief survey”. In: *Electronic Notes in Theoretical Computer Science* 253.3 (2009), pp. 73–82.
- [72] Nicolas Bonneel et al. “Displacement interpolation using Lagrangian mass transport”. In: *ACM Transactions on Graphics (TOG)*. Vol. 30. 6. ACM. 2011, p. 158.
- [73] Ofir Pele and Michael Werman. “Fast and robust earth mover’s distances”. In: *2009 IEEE 12th international conference on computer vision*. IEEE. 2009, pp. 460–467.
- [74] King Davis. “A Global Optimization Algorithm Worth Using”. In: *dlib C++ library*. 2017. URL: <http://blog.dlib.net/2017/12/a-global-optimization-algorithm-worth.html>.
- [75] Jasper Snoek, Hugo Larochelle, and Ryan P Adams. “Practical bayesian optimization of machine learning algorithms”. In: *Advances in neural information processing systems*. 2012, pp. 2951–2959.
- [76] Matthew P Wand, James Stephen Marron, and David Ruppert. “Transformations in density estimation”. In: *Journal of the American Statistical Association* 86.414 (1991), pp. 343–353.
- [77] Jon Herman and Will Usher. “SALib: an open-source Python library for sensitivity analysis”. In: *Journal of Open Source Software* 2.9 (2017), p. 97.
- [78] William E Boyce, Richard C DiPrima, and Douglas B Meade. *Elementary differential equations*. John Wiley & Sons, 2017.
- [79] Walter Gautschi. “Error function and Fresnel integrals”. In: *Handbook of mathematical functions* 55 (1972), pp. 297–308.